CHALMERS
UNIVERSITY OF TECHNOLOGY

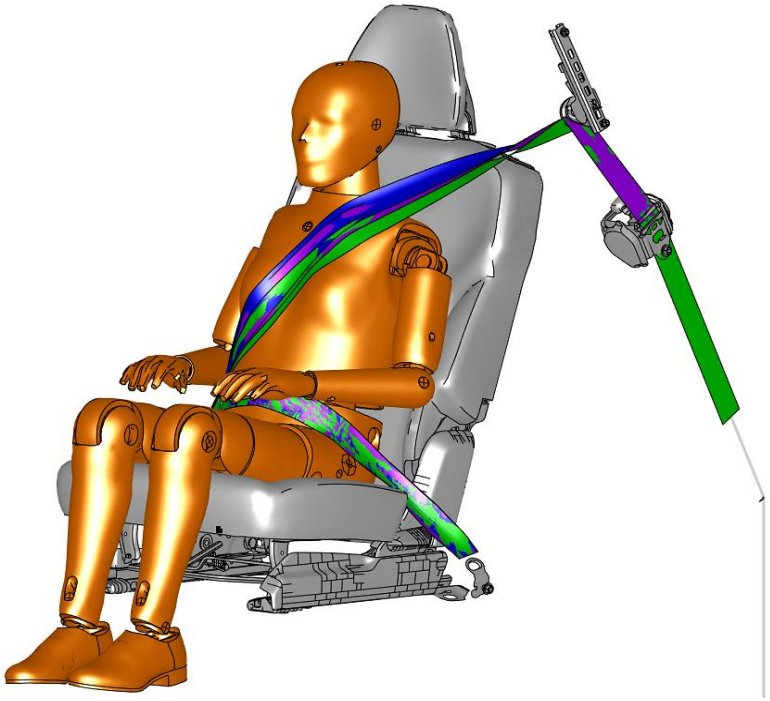

Automation and Standardisation of Seatbelt Routing for Crash Analysis

Additional studies on the influence of the initial shoulder belt position on ATDs and HBMs chest injury metrics in frontal collision simulations

Master's thesis in Mobility Engineering

JULIUS GARD
NICK HAUSWALD

DEPARTMENT OF MECHANICS AND MARITIME SCIENCES

CHALMERS UNIVERSITY OF TECHNOLOGY
Gothenburg, Sweden 2024
www.chalmers.se

Master's Thesis in Mobility Engineering

Automation and Standardisation of Seatbelt Routing for Crash Analysis

JULIUS GARD
NICK HAUSWALD

Department of Mechanics and Maritime Sciences
Division of Vehicle Safety
Chalmers University of Technology
Gothenburg, Sweden 2024

Automation and Standardisation of Seatbelt Routing for Crash Analysis

JULIUS GARD
NICK HAUSWALD

Supervisor: Max Nylund - Volvo Cars Corp., Jobin John - Department of Vehicle Safety
Examiner: Johan Iraeus, Department of Vehicle Safety

Master's Thesis 2024
Department of Mechanics and Maritime Sciences
Chalmers University of Technology
SE-412 96 Gothenburg
Sweden
Telephone +46 31 772 1000

Cover: CAE Model of a Seatbelt routed on a HUMANETICS Hybrid III 5 percentile female Anthropomorphic Test Device.

Typeset in LaTeX
Gothenburg, Sweden 2024

Automation and Standardisation of Seatbelt Routing for Crash Analysis

JULIUS GARD
NICK HAUSWALD
Department of Mechanics and Maritime Sciences
Division of Vehicle Safety
Chalmers University of Technology

Abstract

Crash simulations are a useful method to examine the effect of forces acting in road traffic crashes on vehicle occupants, in order to develop safety strategies based on this. The manual creation of seatbelts in a computational environment is not only very time-consuming, but also deviations in the seatbelt position arise due to the subjective judgment of an individual, lead to difficulties in comparing test results. This study aims to standardise and automate the process of seatbelt creation, significantly reducing the time input while ensuring reproducibility.
The project was carried out using the Finite Element pre-processor ANSA from BETA CAE System. A Python-based automation for creating seatbelts has been developed, which creates a seatbelt within a few minutes for various combinations of vehicles and Anthropomorphic Test Device (ATD) models. The creation of these seatbelt models is reproducible. To evaluate how this unnatural perfection of the seatbelt position compares to a belt routed by a human before a crash test, the deviation in belt position was measured in repeated physical routings for different ATDs. The consequences of this natural lack of reproducibility was investigated by artificially recreating the deviating seatbelts with the automated routing tool and assessing the resulting biomechanical effects in frontal collision simulations.
The developed automation tool has been observed to reduce the time required for creating a seatbelt model to just a few minutes. These generated belt models are reproducible and exhibit no visual variation in their initial belt position. The shoulder belt position can be adjusted based on the input parameter "Mouth to Belt distance" (M2B). The study revealed that the variation in M2B is influenced by the surface shape of ATDs. The convex shape of the Humanetics HIII 50^{th} percentile male resulted in a 95mm difference between the lowest and highest M2B measurement. In contrast, the 5^{th} percentile female benefited from the natural belt guidance provided by the female chest, resulting in a difference of only 45mm between the lowest and highest M2B measurement. Furthermore, the examination of this parameter's spread demonstrated an influence on the chest deflection of ATDs in frontal crash simulations, directly impacting the predicted occupant injury risk. In the case of Human Body Models, which are increasingly crucial in crash simulations, the study determined that the belt position notably affects rib strains and rib fracture probabilities across all age groups. The highest rib strain was observed in the region corresponding to the average position of the investigated belt routings.

Keywords: Vehicle Safety, Seatbelt, Routing, Automation, Standardisation

Preface

This master thesis project was carried out at the Volvo Cars Safety Centre in Torslanda, Gothenburg, Sweden during the spring semester of 2024.

Acknowledgements

First and foremost, we would like to express our gratitude to Chalmers University and the University of Stuttgart. In particular, we thank the respective program directors, Dag Bergsjö and Dr. Bernhard Bäuerle, for their excellent cooperation, which enabled our participation in this exchange and ultimately led to this thesis. Being quickly and warmly integrated into the team is not something to be taken for granted, but it was indeed the case during the completion of the thesis with the Interior Safety Team at Volvo Cars Corporation in Volvo Torslanda.
We would especially like to thank our team manager, Linus Wågström, and our incredibly helpful supervisor, Max Nylund. Our thanks also go to our initial supervisor, Arturo Perèz. Additionally, we extend special thanks to Jonas Östh and Alexandros Leledakis, who consistently provided valuable advice on scientific questions and approaches, and to Peter Appelgren for his unwavering support with ANSA-specific questions.
From Chalmers University, we thank our supervisor, Jobin John, and our examiner, Johan Iraeus, for their helpfulness and guidance. We also extend our sincere thanks to everyone else who accompanied this project over the past five months and made this a wonderful time of learning and experience.

Julius Gard, Nick Hauswald, Gothenburg, June 2024

List of Acronyms

Below is the list of acronyms that have been used throughout this thesis listed in alphabetical order:

AIS	Abbreviated Injury Scale
ATD	Anthropomorphic Test Device
BMI	Body Mass Index
CAE	Computer Aided Engineering
CSV	Comma-Separated-Values
CV	Coefficient of Variation
FE	Finite Element
FEM	Finite Element Method
GUI	Graphical User Interface
H05	Humanetics HIII 5^{th} percentile female ATD
H50	Humanetics HIII 50^{th} percentile male ATD
H95	Humanetics HIII 95^{th} percentile male ATD
HBM	Human Body Model
HPC	High Perfomance Computing
ID	Identification Number
M2B	Mouth-to-Belt distance
MPDB	Mobile Progressive Deformable Barrier Test
N2S	Neck to Shoulder Belt Distance
NCAP	New Car Assessment Program
NHTSA	National Highway Traffic Safety Administration
OEM	Original Equipment Manufacturer
ORS	Occupant Restraint System
PMHS	Post Mortem Human Subject
S2L	Shoulder Belt to Lap Belt Distance
SUV	Sport Utility Vehicle
UN	United Nations
WHO	World Health Organisation

Nomenclature

Below is the nomenclature of indices, sets, parameters, and variables that have been used throughout this thesis.

Δt	Time step size limit
l_c	Characteristic length of the element
ρ	Material density
ν	Poisson's ratio of the material
E	Young's modulus of elasticity
β	Pelvis Angle
l_{sh}	Sitting Height

Contents

List of Figures

List of Tables

1
Introduction

For several decades, our planet's cities have been experiencing an increase in the size and formation of megacities. Consequently, the United Nations (UN) has established 17 goals for sustainable development, including Goal 11, "Sustainable Cities and Communities". This encompasses the aim of making cities and human settlements more inclusive, safer, resilient, and sustainable. As part of this initiative, the number of injuries and fatalities from traffic accidents is intended to be halved by 2030 [Daniel 2015]. The most recent data from the World Health Organization (WHO) shows that approximately 1.19 million individuals die in traffic accidents every year globally. This suggests that despite advancements in comparison to 1.25 million traffic fatalities in 2015, progress is lagging behind the goal [World Health Organization 2016]. However, it is not just fatalities that must be prevented; between 20 and 50 million people sustain injuries due to road crashes annually. Among them, 30% are occupants of four-wheel vehicles [World Health Organization 2023].
In the mid to late 1900s groundbreaking inventions such as the 3-point seatbelt or the airbag were great improvements to vehicle safety. With about 60% fatality reduction for passenger cars the seatbelt is still the single most effective safety system in a crash [Kahane 2018]. Its direct and immediate contact to the occupant is the main advantage and is what made further developments like the belt pretensioner so effective. Such inventions have the capability to better control the accelerations and consequently the forces on the occupants over time. However, accelerations can only be controlled and reduced to a limited extent for physical reasons, which is why vehicle safety has reached a point where further improvements have become a matter of subtle tuning of various safety systems.
Finding a favorable alignment of these interior safety systems requires extensive testing, which is resource-intensive and time-consuming. For this reason, crash simulations have been utilised since the late 1900s, involving modeling of the physical vehicle along with its occupants and safety systems, which are then tested under various load cases. The modeling process is time-consuming, and especially for parts that are frequently changed and must be manually created, it can be a source of deviations in simulation results due to the lack of reproducibility. Additionally, it is reasonable to assume that there is a deviation in the initial position of the seatbelt, both during manual creation and physical application, which impacts the predicted risk of injury. Although current regulations for test setups prevent reducing deviations in physical seatbelt routing [European New Car Assessment Programme 2021], it is possible to standardise the seatbelt position in Finite Element (FE) simulations. This standardisation can enhance the correlation between physical and simulated crash tests by reducing the margin of error on the simulation side.

1.1 Objective

This study aims to develop a solution for achieving reproducible seatbelt models, including their routing position, through standardisation and automation in FE model creation. Additionally, the automation is intended to significantly reduce the time required for seatbelt modeling, thus achieving a more time-efficient process. The developed tool will be implemented in the FE pre-processing tool ANSA and aim for broad applicability across diverse vehicle types and occupant models. Additionally, it will prioritize user-friendliness to enhance ease of utilisation. Furthermore, it should be easily expandable to ensure usability in the future.
In physical seatbelt routing, there are variations in the position of the shoulder belt due to a lack of standardisation and subjective human perception. To achieve a better correlation between physical and simulated crash test results, this study also aims to examine the degree of variation in shoulder belt positioning and its biomechanical impact. Based on data collected during this study, the goal was to determine ans define an average shoulder belt position for occupant surrogates. The seatbelt routing automation should be capable of enforcing this position while also allowing controlled variations from the nominal position.
Additionally, a simulation study will be conducted to examine the variations in shoulder belt positions identified in the physical tests, to establish an uncertainty range for ATD models, and HBMs. This will quantify the possible differences in injury criteria between the simulated crash tests and the hardly reproducible physical crash tests.

1.2 Scope

In this research, a standardised process for seatbelt modeling is developed using existing seatbelt models for various vehicle and occupant configurations of an Original Equipment Manufacturer (OEM) in a FE environment. Subsequently, this standardisation is utilised to create a tool that automatically generates simulation-ready seatbelt models for any combination of vehicle and occupant models within the OEM's portfolio. This encompasses all seating positions, including the most frequently used ATD models as well as HBMs.
To ensure that the generated seatbelt models maintain a representable position towards the average physical routing, a study is conducted wherein a seatbelt is routed on three physical ATDs, ten times each. The objective is not only to determine a suitable and quantifiable belt position for occupant models but also to assess the variability observed in physically routing a belt.
Using the insights gathered from this study, the automated process will generate belt models that position the belt in a manner reflective of its average position after a test engineer routes a physical seatbelt prior to a crash test. Additionally, the impact of this physical variability, and thus the influence of different shoulder belt positions on chest compression, will be examined through simulations to assess the sensitivity of both ATD models and HBMs.

2
Theory

Road crashes can be divided into three phases displayed in Figure 2.1. The pre-crash phase starts when a potential danger arises and ends when the collision begins. The primary objective of the pre-crash phase is to either prevent the collision or to at least reduce the impact and its repercussions. This can be achieved through a variety of methods. For example, driver education and warnings can ensure that drivers accurately recognise potential dangers and respond appropriately. Infrastructure elements such as traffic lights are also utilised to regulate traffic flow and prevent collisions resulting from intersecting trajectories. Additionally, modern vehicles are required to incorporate integrated active safety systems, such as a lane-keeping assistance or automatic emergency braking, capable of detecting and responding to impending danger [European Union 2019]. At a certain point, still in the pre-crash phase, a crash can no longer be avoided, but only mitigated. Active safety systems now aim to minimise the impact of the crash, reducing the risk of injury for the involved people. This can, for example, be achieved by emitting an acoustic signal to alert occupants to brace for impact. Numerous additional technologies have been developed to further enhance safety during the mitigation phase of a crash. While some of these technologies may be classified as more passive safety-oriented, and others as more active safety-oriented, the transition from active to passive safety is considered to be seamless.

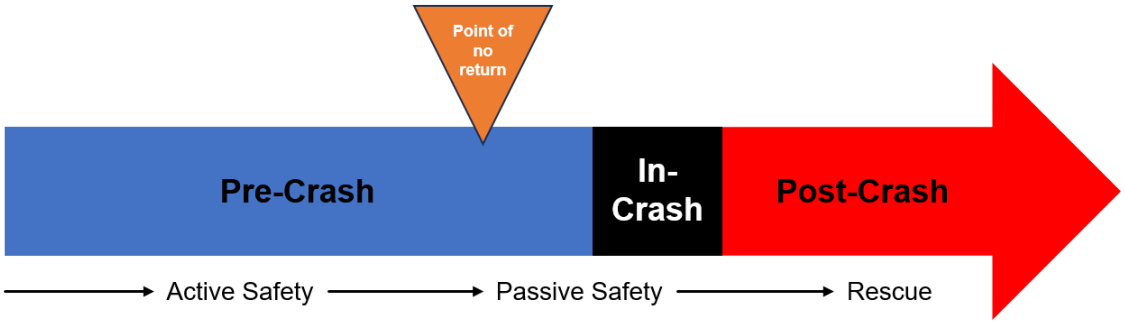

Figure 2.1: Timeline of Crashes

The in-crash-phase often lasts only a few tenths of a second. However, during that time, forces of up to several hundred kilonewtons need to be distributed in a way that keeps the passenger compartment intact and decelerates the occupants inside in a manner that minimises their risk of injury. The body structure of the vehicle has a crucial role in this regard, as it allows targeted deformation in specific areas to minimise the resulting acceleration on the occupants, while simultaneously

maintaining enough structural integrity to prevent intrusions into the passenger compartment. Additionally, restraint systems such as the airbag and seatbelt have been developed to influence the movements of occupants inside the vehicle in a way that minimises the risk of injury. The seatbelt for instance is pyrotechnically pretensioned at the beginning of the in-crash-phase to reduce slack in the belt and therefore reduce deceleration spikes with initialising force on the torso earlier.
After the in-crash-phase, the goal is to keep the vehicle in an uncritical situation and to make a rescue of the eventually injured individuals as fast as possible. A system that counts into this post-crash-phase and is now mandatory for passenger cars on the market is the automated emergency call.
In the domain of crash safety, it is crucial for car manufacturers to adhere diligently to regulations and guidelines during the production of new vehicles. This ensures that the vehicles meet the necessary standards for street legality and registration eligibility. Europe has a system of type-approvals which means that the government is actively checking whether the car complies with all legal requirements for its specific market and issues approvals. These checks usually consist of compliance tests. If a car fails to pass the compliance certification, the process of fixing the issues can be very ressource intensive for the manufacturer in the matter of money and time. Additional non regulatory assessment programs such as the New Car Assessment Program (NCAP) exist for multiple continents and regions. While NCAPs are usually not a governmental institution, they offer guidelines for vehicle crash testing and issue a crash rating which can be used to assess a vehicles crash performance and promote its safety capabilities. Notable NCAPs include [Pereira and Callaghan 2013]:

- USNCAP (United States New Car Assessment Programme): It was founded in 1978 as the first of its kind and is since run by the National Highway Traffic Safety Administration (NHTSA). It is responsible for the US-American market.
- Euro NCAP (European New Car Assessment Programme): Founded in 1997, it provides safety rating for the European market.
- ASEAN NCAP (Association of Southeast Asian Nations New Car Assessment Program): Responsible for the Southeast Asian market.

As in different regions not only the streets, and traffic rules vary, but also the culture and average human body sizes, the test protocol of the different NCAPs often have slightly different safety requirements and test procedures.

2.1 Crash Testing of Cars

To evaluate the crashworthiness of vehicles, they undergo crash testing. Generally, a crash test involves a collision between a vehicle and an obstacle, which could be another vehicle, a barrier, a pole, or any other significant object used to assess crash performance. These tests are conducted in a controlled environment that closely mimics real-world crash scenarios. Both the vehicle and the obstacle, or either one, are accelerated to a specific velocity, additionally the crash is executed at a predetermined angle and contact point. The cars are equipped with sensors that measure for example, acceleration, force, strain or pressure. Additionally video tracking markers

are applied and traced during the crash using high speed cameras. Both is done to extract information about in-crash forces and movements, since humans are not able to process those in the 200 milliseconds of the collision. To evaluate and compare vehicles, the earlier introduced NCAPs developed standardised crash procedures. The following crash tests are performed during the Euro-NCAP assessments for adult occupant protection [European New Car Assessment Programme 2023]:

- Mobile Progressive Deformable Barrier (MPDB): The test car is driven at 50 km/h and with 50% frontal overlap into a deformable barrier mounted on an oncoming 1400 kg trolley, also, travelling at 50 km/h. This results in a relative initial crash velocity of 100 km/h.
- Full-width rigid barrier: The car is driven at 50 km/h into a rigid barrier with full overlap.
- Side mobile barrier: A deformable barrier is mounted on a trolley and is driven at 60 km/h into the side of the stationary test vehicle. This test is performed at different angles.
- Side pole: The test car is propelled sideways at 32 km/h against a rigid, narrow pole.

Since crashing a vehicle for each safety test is a costly process, car manufacturers often conduct procedures that do not require such close resemblance to real-life crashes using sleds. These tests are used for internal development to assess the crash performance of interior components, but they cannot compensate a standardised fullscale test as a final evaluation. Hydraulic sleds, as one can be seen in Figure 2.2, are frequently utilised to judge occupant restraint systems under simplified circumstances.

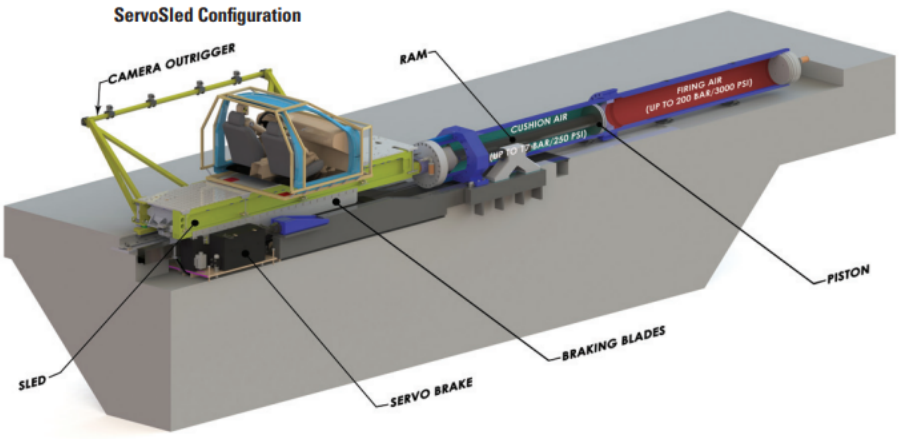

Figure 2.2: Hydraulic sled for testing of occupant restraint systems [Seattle Safety 2018]

2.2 Anthropomorphic Test Devices and Human Body Models

In the 1950s researchers began to investigate on injury biomechanics of occupants in car collisions to correctly assess the actual injuries and their cause. The first surro-

gates for car occupants in crash tests were Post Mortem Human Subjects (PMHS) as well as animals and volunteers. Even though this approach provided highly valuable data, it was quickly abandoned due to ethical and moral concerns. Through technological improvement, ATDs, commonly known as crash test dummies have been developed, trying to closely replicate the biomechanical characteristics of a human body. They are robust, and provide reproducible data on forces, accelerations, displacements and other information that can be collected during a crash test. ATDs are still in use everyday at crash testing facilities and their anthropomorphism is steadily increasing thorugh technological advancements. Different sizes have been developed, the most commonly used are the 5^{th}-percentile female as well as the 50^{th}-percentile and 95^{th}-percentile male, each portraying corresponding mass and proportions of the respective human group. Apart from the physical devices, detailed numerical models have been created representing the dummy in the crash test simulation, they are further referred to as ATD models. Since the 1990s HBMs are being developed. They are computer powered models which more closely resemble the human anatomy as well as its biomechanic and the predicted injury risk in different conditions. HBMs provide a detailed representation of a humans internal structure which can be useful for analysing causes of injuries. Another significant benefit of HBMs lies in their ability to measure forces from all directions, as well as the resulting strains, making them suitable for front, side and rear impacts [Xu et al. 2018]. As an example, Figure 2.3 shows two mid-sized biomechanical models, one physical ATD (a) and one simulation based HBM (b).

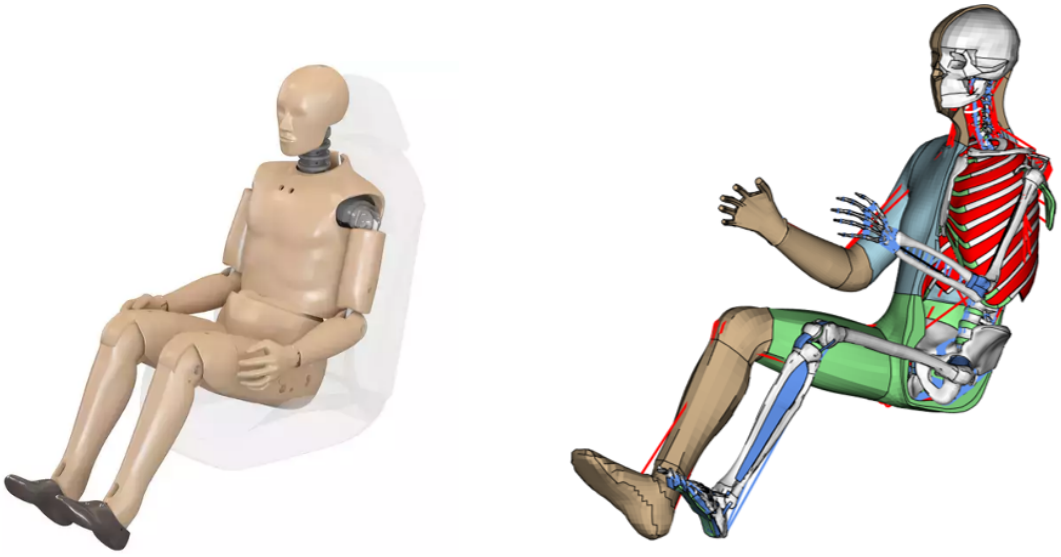

(a) ATD: Humanetics Hybrid III 50^{th} percentile male [Humanetics 2023]

(b) SAFER HBM [SAFER 2022]

Figure 2.3: Biomechanical crash test models

In Euro-NCAP crash tests, the chest criteria for Humanetics HIII ATDs is chest deflection. Chest deflection is defined as the relative change in distance between the ATD's sternum and spine. As the chest is being compressed, this distance therefore changes. In Euro-NCAP crash tests, the maximum chest deflection throughout the

crash is the relevant value that will be used to assess the chest injury criteria. It is calculated according to equation 2.1 [European New Car Assessment Programme 2020].

$$D_{chest} = \max(D_{chest}(t)) \tag{2.1}$$

The Humanetics Hybrid III family uses a chest deflection transducer, as shown in Figure 2.4. It consists of a plate representing the sternum and a ball in the sternum slider that is attached to a beam. As the sternum is displaced, the ball slides up or down in the slider, changing the angle of the beam to which it is attached. This angle is then used to calculate the chest deflection [Humanetics 2017].

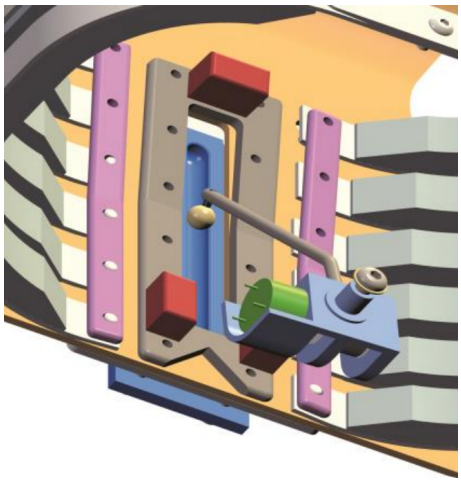

Figure 2.4: Humanetics Hybrid III chest deflection transducer mechanism [Humanetics 2017]

HBMs offer various approaches to examining the probability of chest injuries. One commonly used method is to measure the strain on each individual rib and then relate this strain to injury probability based on data [Larsson, Blennow, et al. 2021].

2.3 Seatbelts as occupant restraint systems

In order to prevent or minimise injuries of the car passengers during a crash, occupant restraint systems (ORS) have been developed. The first ORS being invented was the seatbelt. Its origin can be traced back to the late 1800s, developed by the American Edward J. Claghorn to keep tourists safe in the taxis of New York City. Though it was not until the mid 1930s when several scientists began testing seatbelts and urged manufacturers to provide them in all cars due to their positive impact. The real breakthrough with seatbelts came 1958 when the Swedish engineer Nils Bohlin invented the three-point belt. Its improvement to the single lap belt is, that it not only prevents people to get propelled out of cars, but also to reduce several injury risks by slowing down the torso in the event of a crash. When Bohlin passed away in 2002, Volvo estimated that his invention had saved more than one million lives in the four decades since its introduction. Nowadays, the seatbelt is still the most influencial ORS alongside the airbag [Defensive-Driving 2016].

Figure 2.5 shows a typical modern 3-point seatbelt routed in the driver's position.

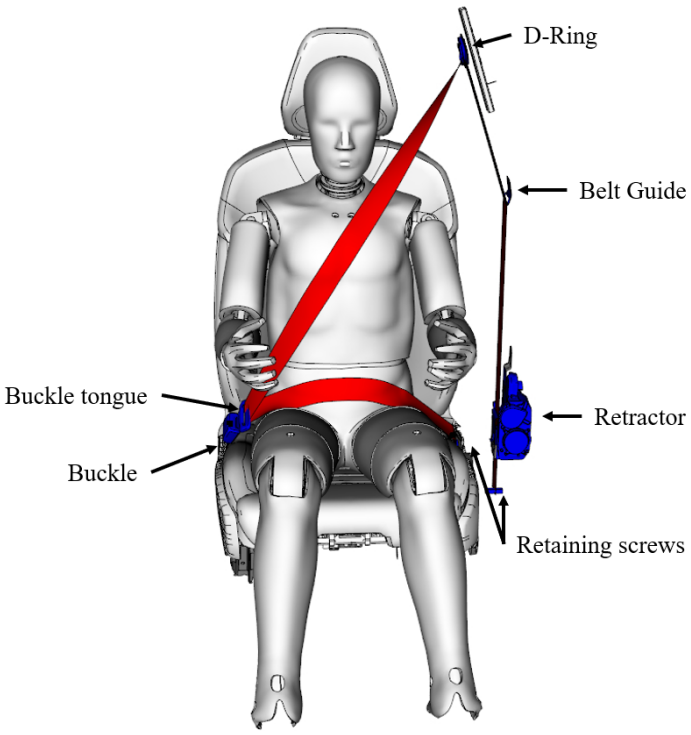

Figure 2.5: Example of a 3-point belt system on the driver position

While the geometric configuration of the belt path depends on the manufacturer's models and the seating position in the vehicle, the whole system usually consists of the following parts:

- The seatbelt itself is usually made of a high tensile yarn in order to be able to withstand high forces during a crash
- A retaining screw fixates the start of the belt to a secured car part.
- A buckle is also attached to an immovable car part to secure the belt on the opposite side of the seat.
- A buckle tongue is used to fasten the seatbelt by inserting it into the buckle. The locking mechanism allows the occupant to easily secure and release the seatbelt.
- A D-ring is used on the highest point of the seatbelt to fixate and position the shoulder belt on the occupants thorax. A D-ring is not essential for a seatbelt, as a different type of guidance is frequently used in the rear seats to set the shoulder belt. Nevertheless, it is typical for a D-ring to be installed in the driver and front passenger seat.
- A seatbelt system can have additional components that function as guidances, which define the path of the seatbelt towards its ending anchor.
- Every modern car is equipped with a retractor near the end of the belt path. It tensiones the seatbelt in order for it to wrap the occupants body in a gentle yet secure way to remove slack. The retractor serves as a belt pretensioner in

many modern vehicles, too. The pyrotechnical pretensioning of a belt further reduces the belt slack shortly before a crash in order to enhance the occupant protection.

- Similar to the start of the belt, the end is also fixated with a retaining screw to a rigid part of the vehicle.

A study from 2020 investigated the effect of the seatbelt on the injury risk of the driver. The results are based on the information and 2016-2017 data provided by the Spanish national traffic department "Dirección General de Tráfico". The study found that failure to wear the seatbelt by driver is likely to increase the risk of fatal and severe injury significantly. While the study investigated several factors in combination with the seatbelt use, the results showed that in every scenario the use of a seatbelt significantly decreased the risk of severe or fatal injury. For every age and sex, the use of a seatbelt decreased this risk by atleast 80%[Febres et al. 2020].

2.4 Finite Element Method and Simulation

Annually, car manufacturers invest millions of euros to conduct tests ensuring the safety of new vehicle designs. Even original equipment manufacturers (OEMs) with extensive resources cannot conduct crash tests on more than a few vehicles per day as the process of setting up the test and retrieving all the data from the cars post crash is very time consuming. For those two reasons, manufacturers and software providers designed computational crash test simulations to run before and parallel to the development process. Digital representations of vehicles and occupant models are being created using computer aided engineering (CAE), which closely resemble the properties of their physical counterpart [Gursel and Nane 2010]. The rapid increase in the technology of computer processors enables OEMs to run more than hundred of simulations every day in order to assess the crash performance of vehicle designs or just sections of a vehicle. In the near future, further increase in computational power will allow an even closer resemblance of the models and the simulation environment to the reality.

The simulation technique used for crash tests is the Finite Element Method (FEM), which obtains its name from dividing an object into a finite number of elements that have approximately the same physical behaviours, such as strain, displacement, stress and pressure. The computational effort of the simulation strongly depends on the simplification of this assumption. As equations must be solved for each of these elements, the computational cost rises with dividing the object in a greater number of elements. Nonetheless, the model's accuracy also improves simultaneously. In general, numerical methods, such as the FEM, are methods that use mathematical approaches to approximate problems which cannot be solved analytically [ibid.].

FEM can broadly be classified into two categories [Friswell et al. 1995]:

- The **explicit** FEM is an approach which is usually used for short durational and highly nonlinear simulations, as equations of motions are solved at each timestep and without iterating. It requires relatively short time intervals, which depend among other factors on the element length. A stable timestep

must be chosen according to equation 2.1.

$$\Delta t \leq l_c \sqrt{\frac{\rho(1-\nu^2)}{E}} \tag{2.2}$$

This use of short timesteps makes the explicit FEM useful for crash simulations due to its duration of about 200 ms and it's unlinear behaviour. However, the explicit FEM should not be used for long term investigations, i.e. investigations on the fatigue of materials.

- The **implicit** FEM is an approach that iterates between time steps, making it unconditionally stable even for larger time steps. This characteristic makes implicit FEM useful for solving linear equations and for long-term investigations. However, highly nonlinear short-term processes such as a car crash are not well-suited for implicit FEM.

Elements in FE can be seen as connectors between nodes, which are discrete points that represent specific locations. Depending on the parts being displayed, there are three types of elements that are usually used: Beam elements connect two nodes, they are used for very long and slender parts, which can be simplified as one dimensional. Shell elements are two dimensional elements and represent thin parts like sheet metal. Bulky structures are usually described by three dimensional solid elements [Friswell et al. 1995].

2.4.1 Numerical reproducibility in FE-Simulations

The crash test rating organisation Euro-NCAP is planning to incorporate virtual crash testing into its rating protocol [Ratingen 2020]. The reproducibility of these tests is crucial, relying on two main factors: ensuring repeatability in the model setup and consistency in solving the numerical simulation task. Achieving numerical reproducibility poses challenges, particularly when simulating applied impact biomechanics models like HBMs, which rely on approximations due to computational limitations. Consequently, the reproducibility of results from solving partial differential equations depends on simulation settings and the numerical precision of the solver. The Coefficient of Variation (CV) for crash responses of body parts in HBMs is ranging from 0.3% to 5.7% for full frontal impact collisions [Östh et al. 2021]. The numerical reproducibility of ATD models has also been extensively investigated, with one study reporting a CV of approximately 5% for repeated Hybrid III tests [Foster, Kortge, and Wolanin 1977]. Both studies included seatbelt models, thus their numerical reproducibility is encompassed in the occupant model CV. Seatbelt fit is another influential factor. To ensure reproducible results, the setup of an FE-model should remain consistent, even when recreated from scratch. Achieving consistency in the belt path and properties is essential for repeatability, necessitating standardisation to mitigate the impact of human subjectivity.

2.5 Occupant seatbelt fit

Numerous studies have demonstrated that the shape and dimensions of an occupant's body has a significant impact on both the fit and positioning of the seatbelt.

Furthermore, it has been observed that the body shape also influences the extent to which the torso is restrained during a crash event.
A study conducted in 2023 examined the positioning of shoulder belts for a range of occupant anthropometrics. This study utilised 132 different setups covering variations in occupant stature, Body Mass Index (BMI), sex, posture, and seat positions. These setups were then subjected to crash simulations of frontal and side collision crashes. The findings indicated that tall occupants with a low BMI are more prone to sliding out of the shoulder belt, while shorter occupants with a low BMI are more likely to experience submarining [Leledakis et al. 2023].
Another study from 2023 focused on the sitting posture of adult vehicle occupants over time and its effect on seatbelt fit. This study revealed that passengers with body characteristics such as a larger chest, prominent abdominal fat, or a shorter seated height tended to experience the shoulder belt moving closer to the neck as time progressed. Additionally, some participants in the study intentionally adjusted the belt position for increased comfort, leading to significant changes in belt fit [Makris, Bohman, and Osvalder 2023].
In 2013 a study analysed the effect of body characteristics on the static belt fit. The study found that the position of the lap belt is very dependent on the BMI of the occupant as obese participants were found to position the lap belt fully above the pelvis and an average of 61mm forward of the Anterior Superior IIliac Spine. Age and sex were found not to have a significant impact on the belt fit. The shoulder belt fit is strongly affected by the location of the D-ring as well as the seated height of the occupant [Reed, Ebert, and Hallman 2013].
Similarly, a study from 2012 found that obesity has a significant impact on the lap belt fit. Worsening its position by shifting it forward and upward relative to the pelvis. The initial shoulder belt fit was found not to be significantly affected [Reed, Ebert-Hamilton, and Rupp 2012].
There are no strict rules on how to rout a seatbelt. NHTSA advises to let the lap belt rest across the hips and not the belly, so technically on the pelvis, beneath the iliac crest. The shoulder belt should be routed not underneath an arm, but over the chest and away from your neck, which evenhow still lets room for a variation of about hundred millimetre [NHTSA 2024]. Technically routing the shoulder belt on the upper bodys center of gravity would be reasonable, but determining this measurement is quite effortful. This raises the question of how the initial position of the seatbelt, particularly the shoulder belt, should be adjusted to minimise injury risk in a crash.

2.6 Seatbelts in FE simulations

Due to the rising importance of simulations with higher similiarity to the physical model, ORSs like the seatbelt are also implemented in CAE models. Consequently of its thin shape, seatbelt webbings are usually modelled using membrane elements. Some belt components, without contact to other parts of the model, can also be represented with 1D elements. This simplifies the model without affecting the crash performance accuracy. BETA CAE Systems is a provider for simulation software. One of its flagships, "ANSA" is used in this project as a pre-processor for generating

CAE seatbelt models. ANSA has a tool implemented for creating seatbelt models. Its functionalities include [Beta-CAE-Systems S.A. 2024b]:

- Splitting up the seatbelt in components, such as for instance the lap belt or the shoulder belt, which can have different properties and connectors inbetween.
- The ability to create shell or beam elements, representing a seatbelt component.
- The ability to interactively modify the belt path after its creation.
- Different types of connecting entities with individual assigned features for each belt component [Fransén and Larsson 2015]:
  - *ELEMENT_SEATBELT_SLIPRING: Sliprings are commonly used in areas where the belt is wrapped around a part, resulting in a sharp angle, for example at the D-ring or buckle. A slipring can be assigned with a friction curve or a constant friction value to modify the forces between entering and exiting belt components.
  - *ELEMENT_SEATBELT_RETRACTOR: The retractor pulls back the seatbelt webbing to reduce slack and to maintain a slight tension.
  - *ELEMENT_SEATBELT_PRENTENSIONER: The pretensioner tightens the belt during the initial milliseconds of a crash. The tool is able to create to replicate the pyrotechnical reel-in process [Livermore Software Technology Corporation 2024].
- The ability to automatically create up to two cross section sets per belt component which can be used to evaluate belt forces during the post-processing.
- The ability to tension each component to reduce slack and ensure its positioning on the corresponding part to wrap.

All of these options can be accessed via the script using ANSA's integrated Python module. The outputed belt file can be read by a solver with the keyword *ELEMENT_SEATBELT_[...].

2.6.1 Belt routing

When routing a seatbelt in ANSA as it can be seen in Figure 2.6, the first step is to select the parts that shall be wrapped. The parts not being selected either do not interfere with the desired path or will be penetrated by the seatbelt. Although the amount of parts being relevant to wrap can vary, the surface layer of the ATD models thorax and pelvis, as well as parts of the seat that are in contact with the seatbelt, should always be selected.

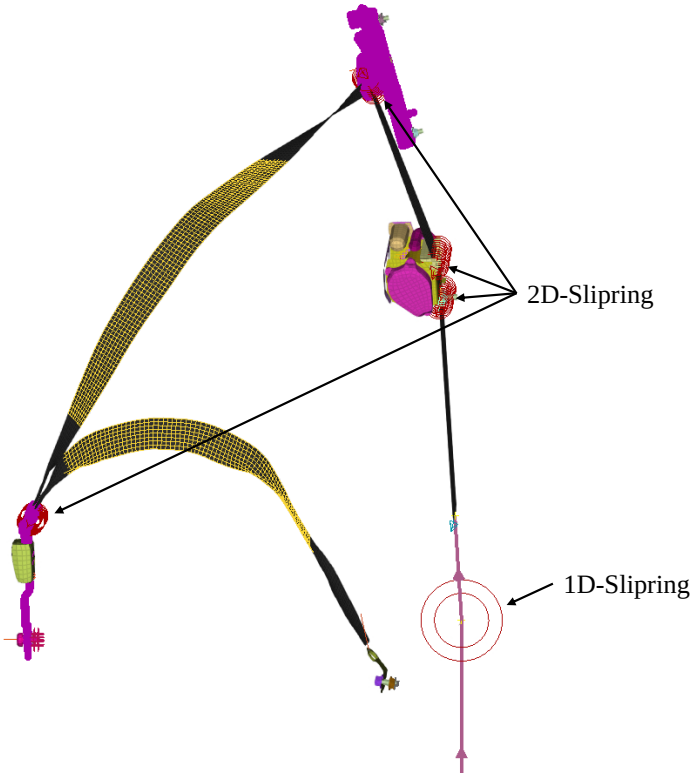

Figure 2.6: Created Ansa Seatbelt with 1D Seatbelt ending

In order to create a seatbelt component, nodes must be selected to define its path. For instance, the path of the shoulder belt can be defined using a node on the buckle tongue, a node on the occupant surrogate model's thorax and a node on the D-Ring. Each component necessitates a minimum of two nodes, specifying the starting and ending points. To provide more precise guidance for the belt, multiple additional points can be inserted in between. These points can be fixed in their positions, independent of interactive modifications and tensioning options. The initial path node of a component must always align with the final node of the preceding component to ensure subsequent joining.

Two components are joined by assigning a connector to the respective end. The commonly used anchor is a Slipring which is shown in Figure 2.7.

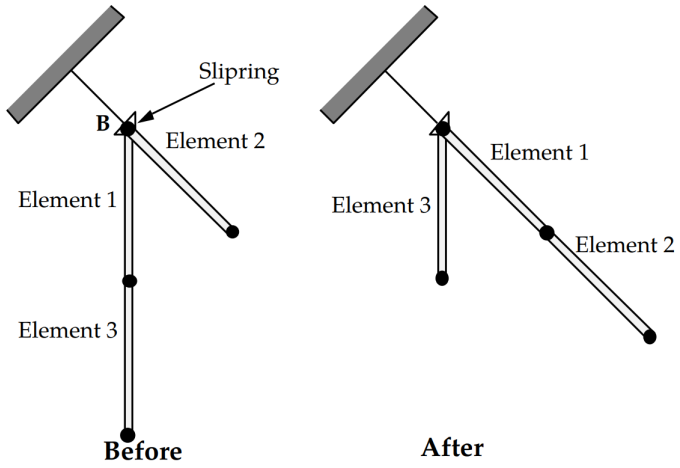

Figure 2.7: Functionality of seatbelt slipring in LS-DYNA [Livermore Software Technology Corporation 2024]

There are several additional attributes that can be assigned to each component, for instance the cross-section distance towards the start and end, the offset to the wrapped parts as well as the number and element length resulting in the width of the belt. Once a part is defined correctly, ANSA displays the created component and opens the interactive editing mode if desired. This provides the possibility to flip the orientation of the belts faces at the endings and move certain points on the intermediate belt path. After the correct position is confirmed by the user, the belt component is finalised.

2.6.2 Belt tensioning

After a belt component is created, ANSA has a built in way of fitting the belt around the wrapped part, resembling the retractor tensioned lap belt path in a physical routing. The option to tension the seatbelt provides the opportunity to "pull" on the start or end of the belt, adapting it to the occupants surface shape. This can be done with a force that is chosen from a scale of one to hundred. Once the process is finished, any previous state that was reached during the tensioning can be chosen as the new definite state of the belt component. The overhanging edges can be cropped and the elements can be smoothened.

2.6.3 Deviation of the belt position

Ensuring optimal seatbelt placement is crucial for safety in vehicle crashes. Inappropriately positioned seatbelts, whether too high or too low, can compromise their effectiveness. A seatbelt positioned too high may apply excessive pressure on the neck during impact, while one placed too low might fail to adequately restrain the upper body and could even cause abdominal compression.
Throughout normal driving, seatbelt positioning may fluctuate due to dynamic driving forces or manual adjustments by occupants. Additionally, initial seatbelt routing may impact its performance. Despite its importance, research on these initial po-

sitions remains limited, especially regarding their influence on crash test outcomes and vehicle safety ratings.
In crash tests, engineers carefully route seatbelts to ensure proper fit. The exact position however is up to their subjective evaluation. This subjective judgment applies both to physical crash tests and computer simulations. Consequently, variability in seatbelt routing, resulting from individual interpretation, can lead to inconsistent results, necessitating attention in academic discourse and practical application.

2.6.4 Mouth to belt distance

The Mouth to Belt distance, as marked in Figure 4.4(a), is defined as the vertical distance between the dummies central mouth node and the lower edge of the shoulder belt. In order to closely resemble the belt path of a physical belt routing, this distance should approximately be the same in CAE models. This distance influences the predicted injury risk [Larsson, Östh, et al. 2024]. The reason for this is that the Humanetics HIII chest deflection transducer measures the relative displacement of the ATD's sternum to the spine box only [Shah et al. 2014]. This means that a belt position which does not primariliy load the ATD's sternum produces a lower chest deflection and therefore a lower predicted injury risk. HBMs on the other hand have a detailed ribcage with all ribs being modelled. Therefore, a deeper investigation can be done on how the belt is routed over the ribcage and how each rib is strained during a crash test simulation. Studies show that the shape and size of the rib cage has a big influence on the predicted probability of rib fractures [Larsson, Östh, et al. 2024]. However, the influence of the vertical shoulder belt position on the HBMs predicted probability of rib fractures has received little attention in research.

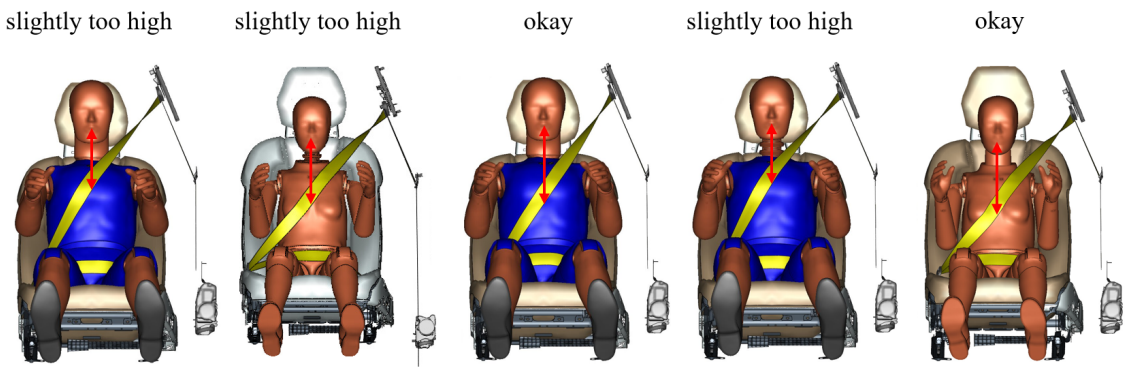

Figure 2.8: Variation of mouth to belt distances on shoulder belt routings for Humanetics HIII ATDs

3
Methods

The project was carried out in a systems development cycle, as depicted in Figure 3.1 of the V-Model. The V-Model was considered a sensible approach here, as it involved continuous verification of requirements, allowing early quality assurance of the final product. It is a standard procedure in software development. Initially, requirements for the final product were gathered before a standardised process was developed for routing seatbelts to meet these requirements. In order to accomplish this, a framework of Python code was created, containing multiple substructures for the individual tasks of automation. Once these substructures were developed, their functionality was continuously checked until the automation was fully functional. The functionality was then verified using different seat positions in various vehicle models to check for standardisation. In the final step, the initially defined requirements were validated, and investigations into the possibilities and limitations of the end product were conducted.

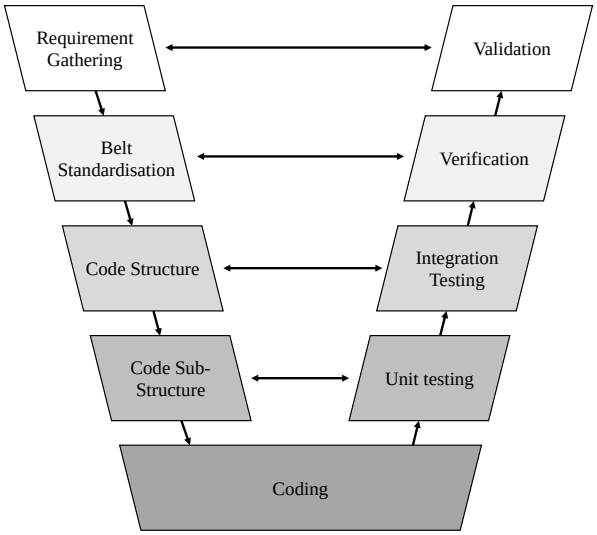

Figure 3.1: V-model illustrating the development process of the automated belt routing tool

All simulations were run on a distributed Linux High Performance Computing (HPC) system at the Volvo Cars Safety Center using LS DYNA version 12.1.0 (ANSYS/LST, Livermore, CA, USA) as a solver. The HPC cluster consisted of

five servers, each with eight to fourteen Intel Xeon processors. For each simulation 256 cores were used for seven to nine hours. The server it was carried out on was not specified.

3.1 Requirements for seatbelt routing

The current situation in many companies conducting occupant protection simulations is that the CAE engineer manually routes a seatbelt in their CAE environment. Therefore, the process of creating a seatbelt model that complies with the simulation requirements is very time-consuming and prone to errors. Consequently, a key requirement was to reduce the time needed for routing a seatbelt. Additionally, when a CAE engineer manually creates the model, standardisation and reproducibility in the process are compromised. This is problematic because variations in belt positioning and parameter configuration can significantly influence simulation results, making it difficult to compare simulations with different belt models. Another requirement was therefore to negate variations in seatbelt position and its properties, thereby increasing reproducibility. Since FE simulations are generally used to replicate physical crashes as accurately as possible, another demand was to investigate the seatbelt's position and its deviation from physical tests in order to find a belt position which closely resembles the average belt position in a physical belt routing. A problem with software development, and thus a continuous requirement, was to ensure its relevance and usability in the future, making sure it remained applicable for future projects, where certain parameters may change. Furthermore, the program had to be easily understandable, making it accessible even to inexperienced users, and its maintenance had to be kept as simple as possible. For this purpose, it was important to integrate clear, unambiguous documentation.
The summary of the requirements can be found in table 3.1.

Table 3.1: Product Requirements

	Requirement
1	Minimise the time required to route a seatbelt in CAE
2	Reproducible results
3	Results shall closely mimic the results of physical tests
4	Extensibility and customisability
5	Clarity and readability of the Python script

3.2 Belt Standardisation

To ensure comparability in crash performance, establishing a standardised process for as many safety systems as possible is crucial, minimising the impact of deviations. An analysis was conducted based on five different FE vehicle models, each equipped with three different Anthropomorphic Test Devices (ATDs), HIII 5^{th} percentile female, HIII 50^{th} percentile male, and HIII 95^{th} percentile male, positioned on the driver, passenger, and three rear seat positions. This analysis aimed to iden-

tify patterns to standardise seatbelt creation with minimal modifications of other submodels. Seatbelts were categorised into four different types of components: the lap belt, the shoulder belt, the belt ending, and numerous additional belt components between the shoulder belt and belt ending that share the same properties. Proper positioning of the lap- and shoulder belts was crucial to ensure correct belt fit on the occupant surrogate, impacting ATD/occupant injury criteria. To achieve this, the path of the lap and shoulder belts was defined by at least three nodes: The start and end nodes of the component, along with an additional node placed at the midpoint of the occupant surrogate's width (horizontal center) at a specific z-coordinate, ensure the correct belt fit. For other components, the exact belt path was less critical as they do not come into contact with the occupant surrogate. Therefore, the belt path for these components was defined only by the start and end node. While the first component, the lap belt, consistently followed the same principle across all investigated belt routings, the ending component was classified into two categories which are commonly used and have a decisive influence the belt setup:

1. The last belt component was a "2D Belt Model" which is a membrane model. In this case cross-sections were applied to this component and it was connected to the pretensioning and retracting mechanism via a "fixed" connection.
2. The last belt component was a "1D Belt Model" and consists therefore of one beam element. In this case cross-sections could not be applied to this component, but therefore had to be applied to the previous one. The end has to be connected to another beam element which was not part of the belt routing include but was connected to the pretensioning and retracting mechanism. The two beam elements were joined with a rigid connection.

Depending on which category a belt routing is applied to, some parameters such as component- endings and anchor types and cross-section positions, needed to be chosen as it can be retrieved from Figure 3.2.

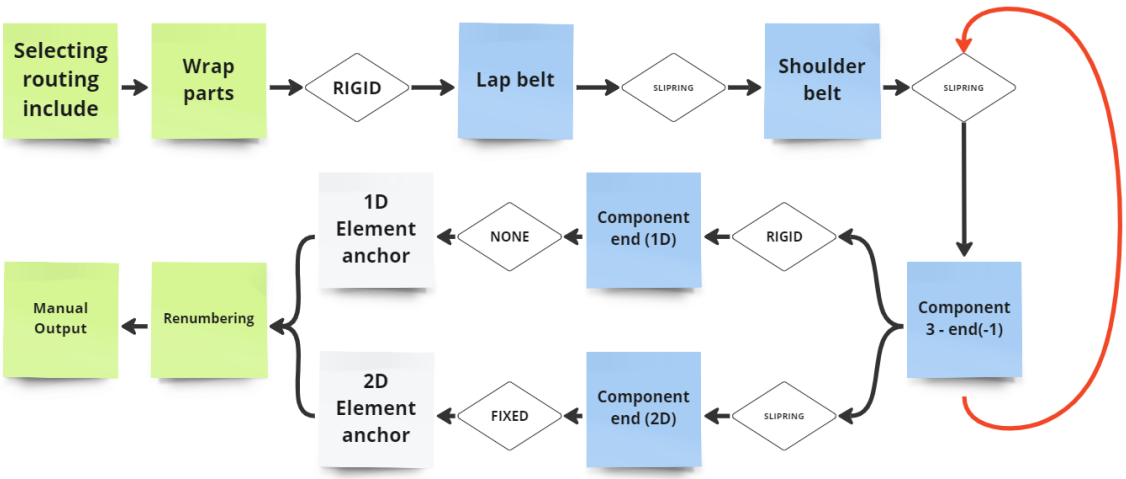

Figure 3.2: Standardised routing flow

Cross-sections are used in CAE to capture belt forces during an impact. Their placement had been standardised, with two cross-sections on the lap belt and two

on the shoulder belt. Each component included one cross-section positioned outside the contact area between the ATD and the belt to mitigate the influence of friction on belt force. Since the contact area varied based on ATD size, the exact position of the third cross-section near the shoulder was deviating, requiring modification depending on the dummy. The adjustment was achieved by measuring the distance between the ATD's mouth and the D-Ring and adapting cross-section placement accordingly. Additionally, one extra cross-sections was affixed to the third component and to the final 2D belt component to measure forces after the D-Ring. Furthermore, belt beams were added to the lap and shoulder belt to add bending stiffness, which cannot be provided by just using membrane elements. The belt beams are positioned both along and transverse to the belt path, situated between the membrane elements. The positioning of the cross-section one to six, as well as the belt beams can be seen in Figure 3.3.

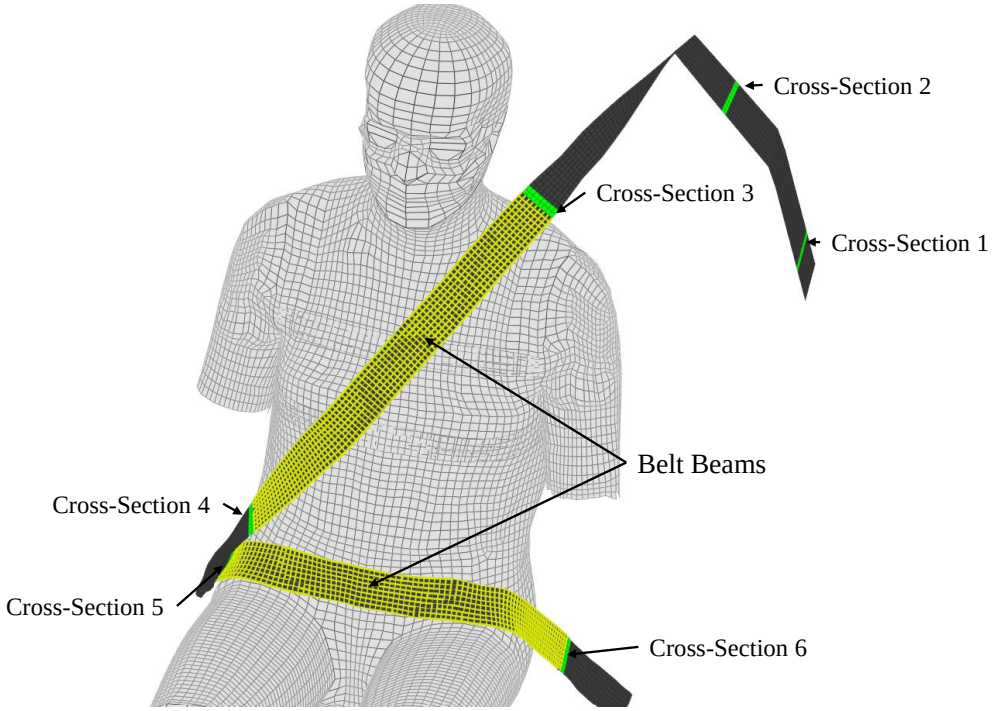

Figure 3.3: Placement of Cross Sections and Belt Beams

However, balancing standardisation and customisability was often challenging which is why some information had to be outsourced. Given the importance of uniformity within a project, certain parameters were deputed and stored in "Comma-Separated-Values" (CSV) files. While this necessitated initial project setup by the user, it also granted them the flexibility to tailor a belt to meet specific project requirements. The resulting CSV file contained information for every belt routing within the project, ensuring standardised belts for each routing instance.

3.3 Automation of seatbelt routing

The process of routing a seatbelt was automated using the Python interface implemented to ANSA, covering the progressive steps of the developed tool, listed in the box of Figure 3.4.

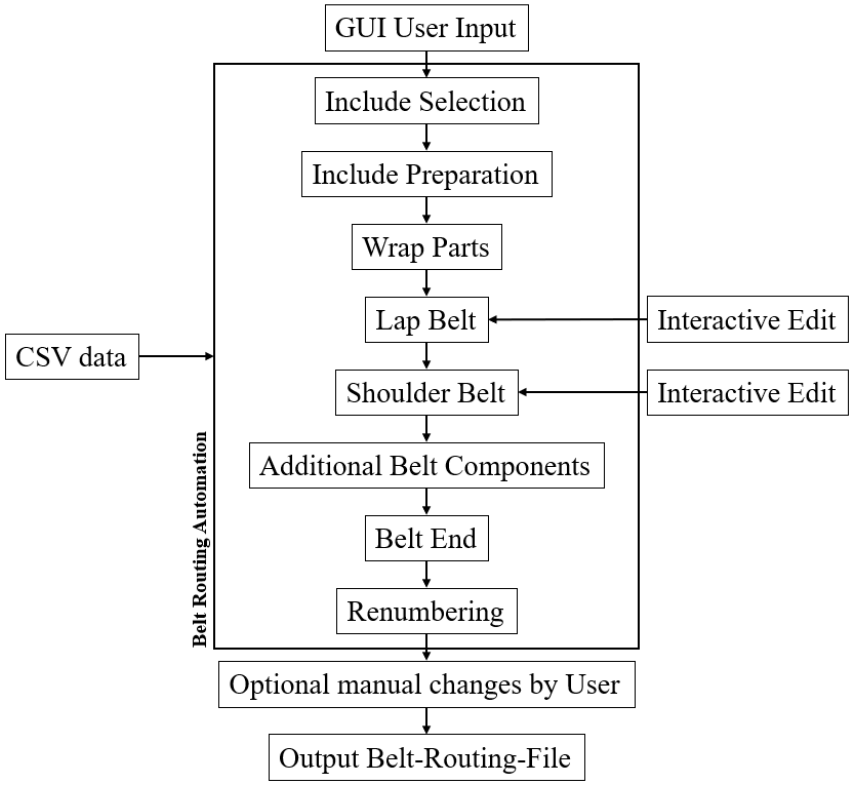

Figure 3.4: Overview of Belt Routing Automation with external influencial factors

The tool is accessible in ANSA through a User-Script-Button named, "Automated Seatbelt Routing". Clicking that button opened the Graphical User Interface (GUI) shown in Figure 3.5. To enhance usability and reduce errors, an Auto-Detection feature has been developed. This feature analysed the names and IDs of models loaded in ANSA to detect the parameters required for the GUI setup. In case of incorrect parameter detection, users have the option to manually adjust them.

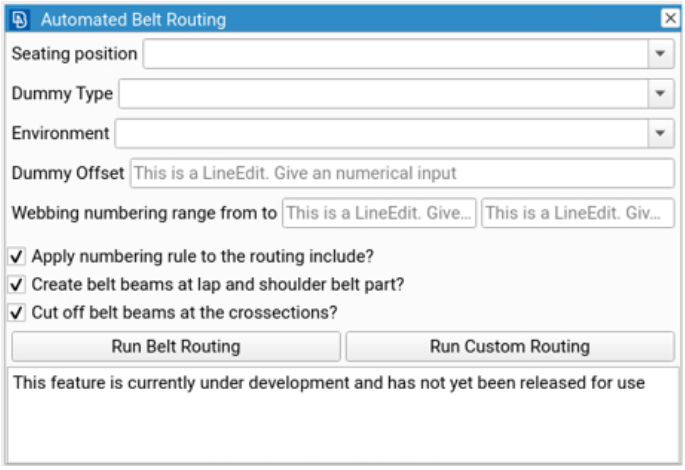

Figure 3.5: General Graphical User Interface for the Automated Belt Routing

As discussed in Chapter 3.2, the routing process relies on various IDs of Nodes, Properties, Elements, and other entities, all stored in CSV files. Those files were accessed by the script based on the input to the GUI. A key focus of development was to ensure the functionality and robustness of the automation even for ambigous inputs. To achieve this, the script prompted user inputs when there was insufficient or excessive information. For example, the selection of the Routing-Include depended on the script identifying an Include containing belt routing entities. If the active model contained none or multiple such Includes, the user was prompted to make a manual selection.
Reducing the time required for belt routing was a primary project goal. However, the belt routing process often began with creating a Routing-Include that lacked a belt webbing but provided necessary anchors and properties later assigned to the generated seatbelt. This process was error-prone and time-consuming, prompting the implementation of a solution within the automation. Therefore the tool enabled users to include a previous belt routing in the model, which was then automatically prepared. Upon identifying/picking the Routing-Include, the automation determined whether the Include was already prepared for a new belt routing by analysing the number of elements in the Include file. If a belt model already existed, the automation deleted corresponding entities, retaining only those necessary for creating a new model.
The ANSA-Python-Interface includes a predefined set of functions within the "ASeatbelt" class, mirroring the options available in the manual ANSA Seatbelt tool. Thus, the initial step in creating the seatbelt automation involved crafting a Python "Belt-Class". The components outlined in the CSV files were encapsulated using the "parts2wrap" function. When constructing the belt components, their path was defined by assigning Node IDs to the belt component via the "set_component_points" function. Standardised component parameters were then assigned using the "set_component_parameters" function before the belt component was created using the "create_component" function. The Interactive-Edit-Mode was exclusively enabled for the lap and shoulder belt, as modifications were unnecessary for the other components not in contact with the occupant model. Given that the M2B was user-defined based on the mouth position, the automation identified a node on

the occupant surrogate's thorax corresponding to the desired distance. This node was designated as a "Known Point" using the "set_known_points" function, ensuring the belt's position at this location remained unchanged and unaffected by modifications made in the Interactive-Edit-Mode or when tensionig the belt component. Once the user had confirmed the modifications, the belt was tensioned based on a standardised process refined through trial and error, as it was observed that excessive tensioning could disconnect the anchors. This tensioning process smoothened the belt path and adapted it to the occupant surrogate's surface shape. The automation exhibited scalability by generating an indefinite number of components, with the creation of the third component to the second to last component executed within a loop. This design granted adaptability to future requirements, as components were generated based on standardised logic outlined and depicted in Figure 3.2.
In the GUI depicted in Figure 3.5, users had the option to execute the routing according to specified parameters by clicking the "Run Belt Routing" button. This action necessitates correctly filled CSV files. Alternatively, users could opt to click on "Run Custom Routing". The Custom Routing served as an alternative development to utilise the standardised routing process, saving time compared to using the default ANSA belt routing tool, and without relying on CSV files. The distinction between routing based on CSVs and Custom Routing lies in the additional parameters required when using the latter. Users are prompted to provide these parameters in a secondary GUI, as illustrated in Figure 3.6. During the routing process in Custom Routing, the user defines the belt path manually by clicking the nodes. Although this process demands more time than the fully automated routing, it offers greater flexibility and the opportunity for research into different belt positions while remaining notably faster than the default ANSA tool.

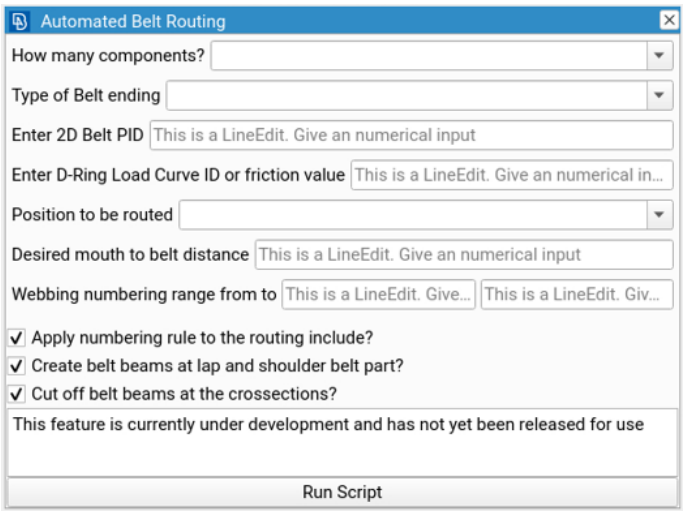

Figure 3.6: Graphical User Interface for the Semi-Automated Belt Routing

The final stage of the Belt Routing entails ensuring compliance of the created entities with simulation and post-processing standards. This step is crucial to ensure the belt complies with simulation requirements and post scripts, which search for specific IDs that must be assigned accordingly. The compliance process includes:

- Assigning the 2D and 1D elements, as well as beams, to a defined property.
- Deleting previously created webbing beam elements outside of the created shoulder and lap belt cross-sections to avoid complications with cross-sections and sliprings.
- Renumbering the cross-sections according to post-processing standards.
- Renumbering sliprings according to post-processing standards.
- Assigning friction values to the generated sliprings.
- Renumbering created entities according to the desired numbering range while not changing pre-defined IDs regardless of whether or not the numbering range contains their ID.

Once the automation is finished the user is provided with an information about the scripts run-time as well as the length of the generated belt webbing, which can be used for post-processing.
The interaction between the four scripts that make up the automation can be seen in Figure 3.7.

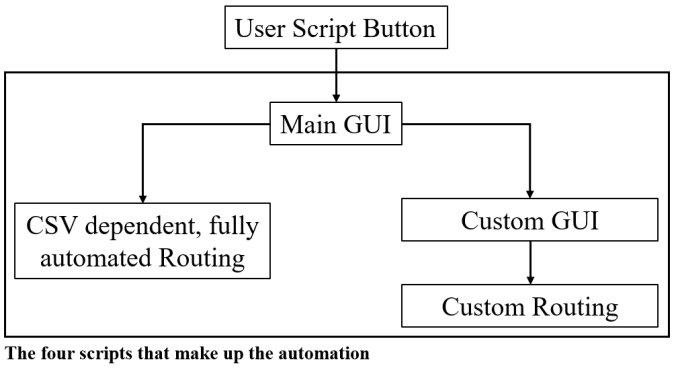

Figure 3.7: Interaction of automation scripts

3.4 Validation of Automation and Standardisation: Performance and Examination of Possibilities

The final stage of the development process involved validating the performance of the created automation and assessing the extent to which it meets the product requirements. This validation process was broken down into several subtasks. Firstly, the automation had to operate as intended, meaning that when executed, the seatbelt was routed according to the desired specifications. Secondly, the performance of the belt and its properties had to align with the simulation requirements to ensure its functionality in CAE-Simulations. Upon successful completion of this validation, it was confirmed that the belt automation functioned as intended. However, the introduction of a new tool also brought new possibilities that could enhance the accuracy and precision of CAE-Simulations. Details on these possibilities were explored in the subsequent chapters.

3.4.1 Validation of Belt Performance

The validation of a subsystem in a simulation proved to be challenging due to the influence of other subsystems on the simulation results. For instance, it was observed that a seatbelt deviating from the physical characteristics of the actual seatbelt could result in dummy forces closer to real forces. This occurred because the discrepancies in belt fidelity compensated for deviations in the fidelity of other subsystems. Consequently, while the overall system improved, the accuracy of the seatbelt-subsystem was compromised. Given the long-term objective of aligning all subsystems of a CAE model as closely as possible with real properties, a validation approach was adopted. Instead of comparing the belt performance with a physical crash test, it was compared with the performance of a seatbelt validated by the manufacturer. To accomplish this, a new seatbelt was created in the same vehicle CAE model, featuring the identical ATD, a V1.5 Humanetics HIII 50^{th} percentile. This seatbelt was placed to closely match the validated seatbelt's position. The positional alignment of the two seatbelt models can be observed in Figure 3.8. Subsequently, a simulation was conducted using the same crash pulse, which was a 35 mph frontal impact according to USNCAP specifications. The seatbelt being compared to was created using the Oasys PRIMER software and is further addressed to as Primer belt.

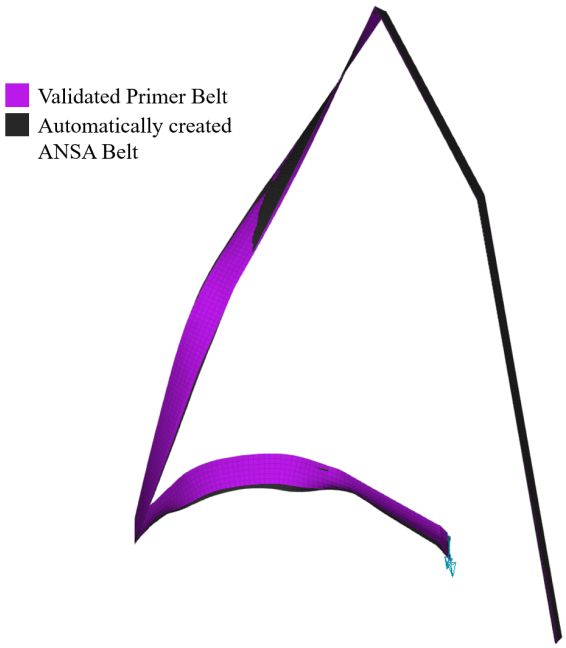

Figure 3.8: Positional overlay of validated Primer belt with automatically created ANSA seatbelt

As a key development goal was to achieve as much reproducibility as possible, a seatbelt was routed two times in the exact same CAE environment with the same positional anchors and parameters. The belts were compared by overlaying them in ANSA to see if the path of the belt may have differed in some areas due to the way ANSA calculated the belt position before and after tensioning the seatbelt.

3.4.2 Deviation in Belt Routing Position for Physical Routing and CAE

Simulations are simplified replications of physical models. Using the developed tool, the seatbelt was routed twice within the identical vehicle model. Since the overlay comparison of the resulting belt models revealed unnoticeable positional deviations in the seatbelt elements, implying that the deviation is less than 10^{-1}mm, and therefore highly reproducible, unnatural perfection was achieved. In reality, when a test engineer routed a seatbelt on a physical ATD, the placement of the seatbelt was at the discretion of the test engineer. According to Euro-NCAP, the belt should have been in a 'natural position' [European New Car Assessment Programme 2021]. This meant that the placement of the seatbelt was subject to the engineer's judgment of what constituted a natural position as it is not quantified. This subjective placement introduced a deviation in the belt position, which was not present in the Automated Belt Routing tool. As part of the validation of the tool, the expected amount of variance was investigated. An assumption was also made that the spread was dependent on the ATD's size and shape, which was why the following was investigated for Humanetics Hybrid III 5^{th} Female, 50^{th} Male, and 5^{th} Male. Successively, each of the physical ATDs was positioned in Position 4 (rear seat, driver's side) of a large sport utility vehicle (SUV). The car and position were chosen due to a configuration of fixed belt points which was considered to be representative of the back seat as well as the front seats. The physical ATDs were positioned according to Euro-NCAP requirements which can be found in Table 3.2 [ibid.].

Table 3.2: ATD-Positioning in large SUV

	H-05	**H-50**	**H-95**
Pelvis Angle	20° (± 0.5°)	22.5° (± 2.5°)	22.5° (± 2.5°)
Head Angle	0° (± 0.5°)	0° (± 0.5°)	0° (± 0.5°)
Y-Alignment	Mid of Seat (± 5mm)	Mid of Seat (± 5mm)	Mid of Seat (± 5mm)
Knee Distance	210 mm	210 mm	290 mm
Arm Position	Fingertip on Knee	Fingertip on Knee	Fingertip on Knee
D-Ring Position	Lowest	Highest	Highest

To position the seatbelt, the physical ATDs were secured, and slack in the lap section was removed with minimal force until the belt gently rested around the pelvis. Next, the shoulder belt section was pulled 50 mm to 100 mm away from the physical ATD's chest and retracted using only the force from the retractor. This process was repeated three times until a belt placement considered natural by the engineer was achieved. As such, the placement was subjective. However, objective criteria ensuring the belt did not "hammock" or buckle on the chest were adhered to. This process was repeated ten times for each physical ATD without moving it. While the majority of routings were performed by the same engineer, up to three other engineers also participated, each routing one seatbelt. This approach was adopted to observe variations in what different engineers perceived as a natural

belt position, while also assessing the consistency when one engineer routed a belt multiple times.

A FARO 8-Axis Quantum ScanArm with a PRIZM Laser Line Probe scanner were used to digitize the seatbelt routings. The first laser scanning for each physical ATD was done to a high degree of detail with reference points on the seat, the ATD, D-Ring, and Buckle which helped align the scannings with the digital vehicle model during the evaluation. The following nine scans included just the important belt parts and the mouth of the ATD as a reference point as the scanned points were transformed to a car model-specific coordinate system.

The seatbelt position in the scannings was determined through three measurements which were acquired using ANSAs Measurement tool:

1. The Mouth-to-Belt-Distance (M2B): The distance between the ATD's middle mouth node and the lower edge of the shoulder belt with the same Y-coordinate.
2. The Shoulder Belt-to-Lap-Belt-Distance (S2L): The distance between the shoulder belt node used for the M2B and the node on the upper edge of the Lap Belts on the X-Z-plane.
3. Horizontal-Neck-to-Shoulder-Belt-Distance (N2B): The distance between the center node on top of the ATD's neck collar to the shoulder belts outter edge which has the same Z-Coordiante as the Neck Collar Node.

The measurements can also be seen in Figure 3.9.

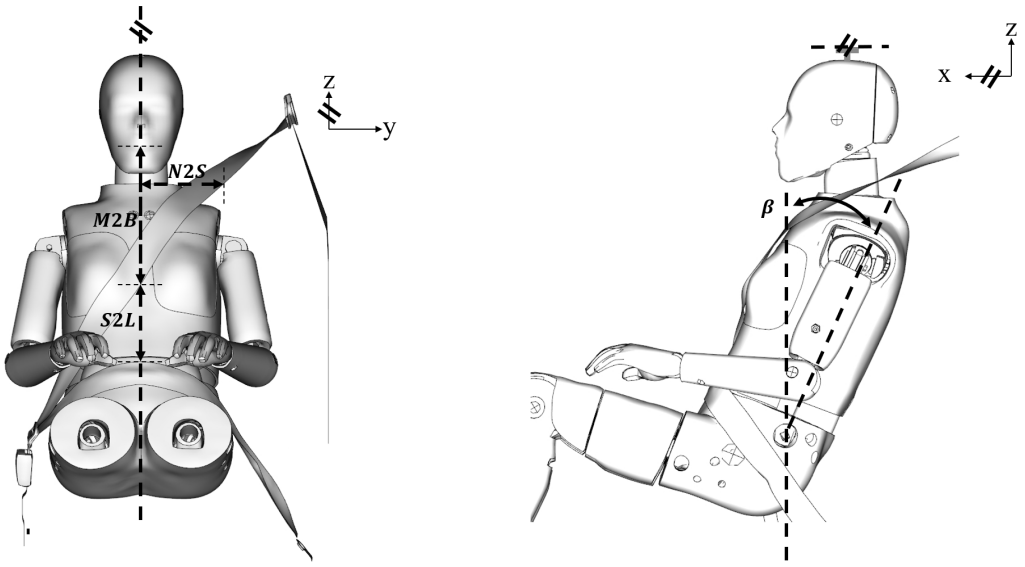

(a) Measurements on Belt Position (Front view)

(b) Measurements on Belt Position (Side view)

Figure 3.9: ATD positioning according to Table 3.2 and belt position measurements

3.4.3 Belt routing on Human bodies

To understand how the M2B and its variation differ between ATDs and humans, four participants were consecutively placed in the same seat and vehicle as the ATDs described in Chapter 3.4.2. Each participant routed the seatbelt on their body ten times. It was decided that the participants should route the seatbelt themselves, as this better reflects real-life scenarios where individuals normally place the seatbelt on their own body. The same measurements as in Chapter 3.4.2 were taken, but this time they were measured physically. This was necessary because a human cannot sit perfectly still for 5 minutes without moving or breathing, which would have affected the quality of the 3D scanning, making it impossible to take accurate measurements. Four male participants were chosen with body proportions slightly above and below those of the Humanetics 50^{th} percentile male, to enable comparison with this specific ATD. The body characteristics of the participants are listed in Table 3.3.

Table 3.3: Deviation of belt position on humans

	H50	**Person 1**	**Person 2**	**Person 3**	**Person 4**
Sex	Male	Male	Male	Male	Male
Seated Height	883.6 mm	826 mm	917 mm	960 mm	968 mm
BMI	NaN	24.28	29.22	23.12	22.92

The measurements were later compared to the ones of the 50^{th} percentile male ATD from Humanetics using M2B boxplots.

3.4.4 Effect of Different Belt Positions on predicted ATD Injury Risk

During a crash, the movement of ATDs and the forces exerted on both the ATD and the seatbelt are expected to depend on the positioning of the belt. Research was conducted to assess the extent to which variations in seatbelt position affect the post processing results. Ten measurement runs were analysed to investigate potential correlations between the measurements. Subsequently, the runs were organised based on their outcomes. Using the previously developed Automated Belt Routing Tool, five specific seatbelt positions were replicated. As the measurements were obtained from a large SUV, the seatbelt models were integrated into a FE car model resembling the physical vehicle used in the tests. To ensure accurate replication, the car model was overlaid with corresponding scans. Components such as the Belt-Buckle, Seat, D-Ring, and ATD were adjusted until the model represented the measurement environment. The seatbelt was then positioned using both the acquired measurements and the overlay of the belt scan, while maintaining consistency in the routing environment to minimise any extraneous factors influencing the simulation's results apart from the shoulder belt position. A new seatbelt model was created five times within the routing environment. These iterations represented the highest and lowest-, the average-, as well as the 25^{th} and 25^{th} percentiles of M2B belt position. The belt models were integrated into the vehicle model and subjected to simulations using a 50 kph MPDB crash pulse and a 25 mph FFRB crash pulse.

These specific pulses were selected due to their simulation of frontal impacts under different conditions, offering the opportunity to investigate consistency in the outcomes. This procedure was subsequently replicated for each of the three ATDs which were previously measured.
While the average M2B served as a standardised parameter in the belt routing automation to guarantee consistent positioning of the shoulder belt, understanding the variability in actual shoulder belt placements relative to simulated injury criteria was crucial. Through comparison of simulation results, uncertainty margins were established to forecast the extent of deviation between the standardised FE-seatbelt outcomes and the physical seatbelt placements.

3.4.5 Effect of Different Belt Positions on SAFER HBM chest injuries

Similar to chapter 3.4.4, variations of shoulder belt positions were investigated using a V10 SAFER HBM representing the 50^{th} percentile male. As HBMs will be a part of NCAP test ratings in the near future, the sensitivity of HBMs to the belt position is something that needs to be assessed in order for the tests to be reproducible. Furthermore, HBMs provide the possibility of a more detailed approach on how the belt position would influence a real human occupant. The HBM was positioned in the same model as the numerical ATDs previously. As the seated height of the SAFER HBM 50^{th} percentile male is very close to the seated height of the Humanetics HIII 50^{th} percentile male, the nominal M2B used was 275 mm. Unfortunately, it is not possible to take the same measurements as in Chapter 3.4.2 for the HBM, since an HBM is a computational model and cannot be placed in a physical car. However, based on the findings regarding the spread in M2B for routing on an ATD, a maximum spread of approximately $\pm$ 30 mm between the nominal M2B and the minimum or maximum position was chosen for this specific HBM, based on engineering judgment. Therefore, 5 simulations with belt positions of M2B average, belt positions of M2B $\pm$ 15 mm and M2B $\pm$ 30 mm were run using a MPDB crash pulse and also a FFRB crash pulse.
The SAFER HBM offers the possibility of analysing the strain on each rib throughout a crash, providing a more detailed approach to investigating the positional effect of the shoulder belt. Rib strain data was extracted from the simulation results using a post-processing script, which outputs screenshots of the rib cage at the point of highest strain and provides detailed values on rib strain. Based on these values, the probability of fractures in 2 or more, 3 or more, and 4 or more ribs was calculated for different age groups (25, 45, and 65 years) using rib strain thresholds combined with age-based factors. The method used in the post-processing is explained in a 2021 study by Larsson [Larsson, Blennow, et al. 2021], originally developed by Forman in 2012 [Forman et al. 2012]. In summary, the rib strain data obtained from the crash simulation using the HBM was compared to the failure strain values of multiple PMHS from various age groups and sexes. This comparison enabled the estimation of rib fracture probability across different age groups.

4
Results

The following chapter presents the results originating from the automation and standardisation of seatbelt creation. Furthermore, it digs into the influence of different seatbelt parameters and discusses the findings of a study on the spread in seatbelt position following initial seatbelt routing and the corresponding effects of this spread. The impacts were examined for both the Humanetics HIII family and the SAFER HBM.

4.1 Seatbelt routing automation

The belt routing automation can route a seatbelt for various combinations of vehicle model and occupant model. This means that the tool has no limitations compared to manual seatbelt routing, other than the chosen standardisations. A seatbelt can be routed on both an ATD model and an HBM, given they both consist of nodes and elements.
The runtime of the script was found to be less than 5 minutes in existing vehicle models. The exact run-time depends on the size and level of detail in the vehicle model, as well as the complexity of the belt path. Manual seatbelt routing, using the ANSA seatbelt tool, requires between 45 minutes for an experienced CAE engineer, who is familiar with the model and the required belt properties, and multiple days for an inexperienced engineer or a first-time model setup. Therefore, the automated tool is a time efficient solution once the vehicle model-specific CSV file is created, which only needs to be done once and was found to take about 10 minutes for each position.
The developed tool allows the user to make manual changes after the belt was created to apply, for instance, different friction values for the sliprings or apply different renumbering rules. Also, all properties assigned to the seatbelt are stored in a seatbelt entity and can be modified after the belt's creation by changing properties in the ANSA seatbelt routing tool, which is automatically filled with properties that are assigned to the belt. While the created seatbelt follows the standardisation which was generated when setting up the CSV, this allows for individual modification which can, for instance, be used for research purposes.
The Custom Belt Routing Tool was found to have a slightly higher runtime of approximately 7 minutes. The reason for this is that the Custom Routing requires a higher amount of user input due to its independence from CSV files. Therefore, the user actively chooses the belt path and assigns properties in the GUI. As this process still follows the same standardisation, it is still a big time saver compared

to the default ANSA tool.

4.2 Seatbelt routing standardisation

For the standardisation of the seatbelts, default values needed to be assigned to belt parameters mentioned in chapter 2.6. The effect of those parameters was investigated to estimate to what extent they impact the results of the simulation. The offset of the belt was found to be neglected by the pretensioning mechanism. This means that the slack of the seatbelt was quickly removed. As Figure 4.1 shows, the displacement curves, which show how much the belt is pulled out of the retractor, are parallel to each other. The result of this, is that the belt forces and the forces and displacements on the ATD do not change depending on the initial belt offset. Therefore, the offset influences only the webbing length which does not directly effect any injury criteria.

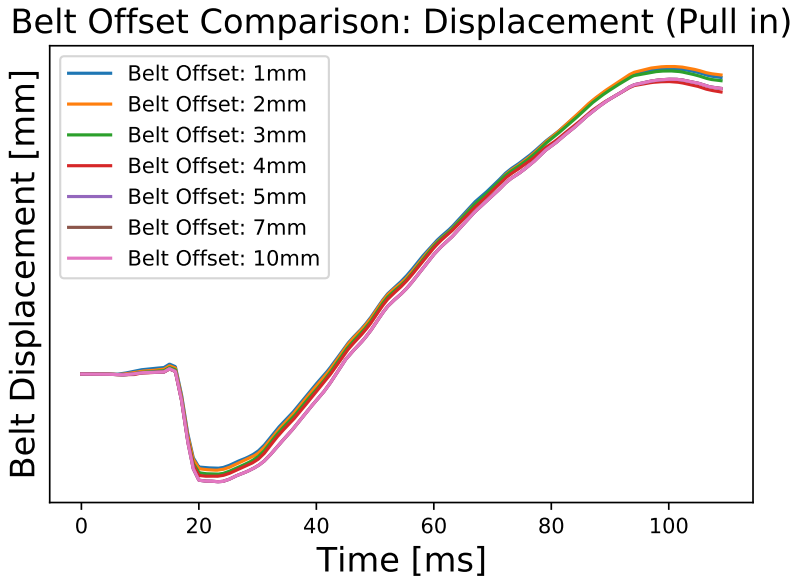

Figure 4.1: Comparison of Belt Displacement based on its Offset to the ATD's surface

The number of belt elements in width, and thus the element size, had negligible influence on the simulation results. Therefore, a quantity of 8 elements in width, each with a side length of 6 mm, was utilised. The computational power required for the creation of the seatbelt model in this configuration is not much greater than with 4 elements at 12 mm each but notably lower than with more smaller elements. Altering the size of the belt webbing elements did not significantly impact the computational power needed for simulations using the belt models as they are a very small part of the overall vehicle model. Element beams were employed alongside the belt webbing in the regions between cross sections 3 to 4 and 5 to 6 to enhance stiffness and minimise noise in the contact zones between the occupant surrogate and seatbelt. While the incorporation of element beams did not affect the quantified simulation outcomes, it did decrease noise.

4.3 Validation and Performance of Routing Automation

Two simulations, which only differ in their belt model, were compared. One belt model was created with the PRIMER software and is considered to be validated against a physical belt following previous non published work at the manufacturer's facilities. The other belt model was created using the Automated Belt Routing Tool in ANSA. The comparison in several deciding plots for the belts performance can be seen in Figure 4.2. The belt seemingly reacts to forces the same way, the Primer belt does. The Auto-created belt follows the curves of the Primer belt closely with only some marginal deviations.

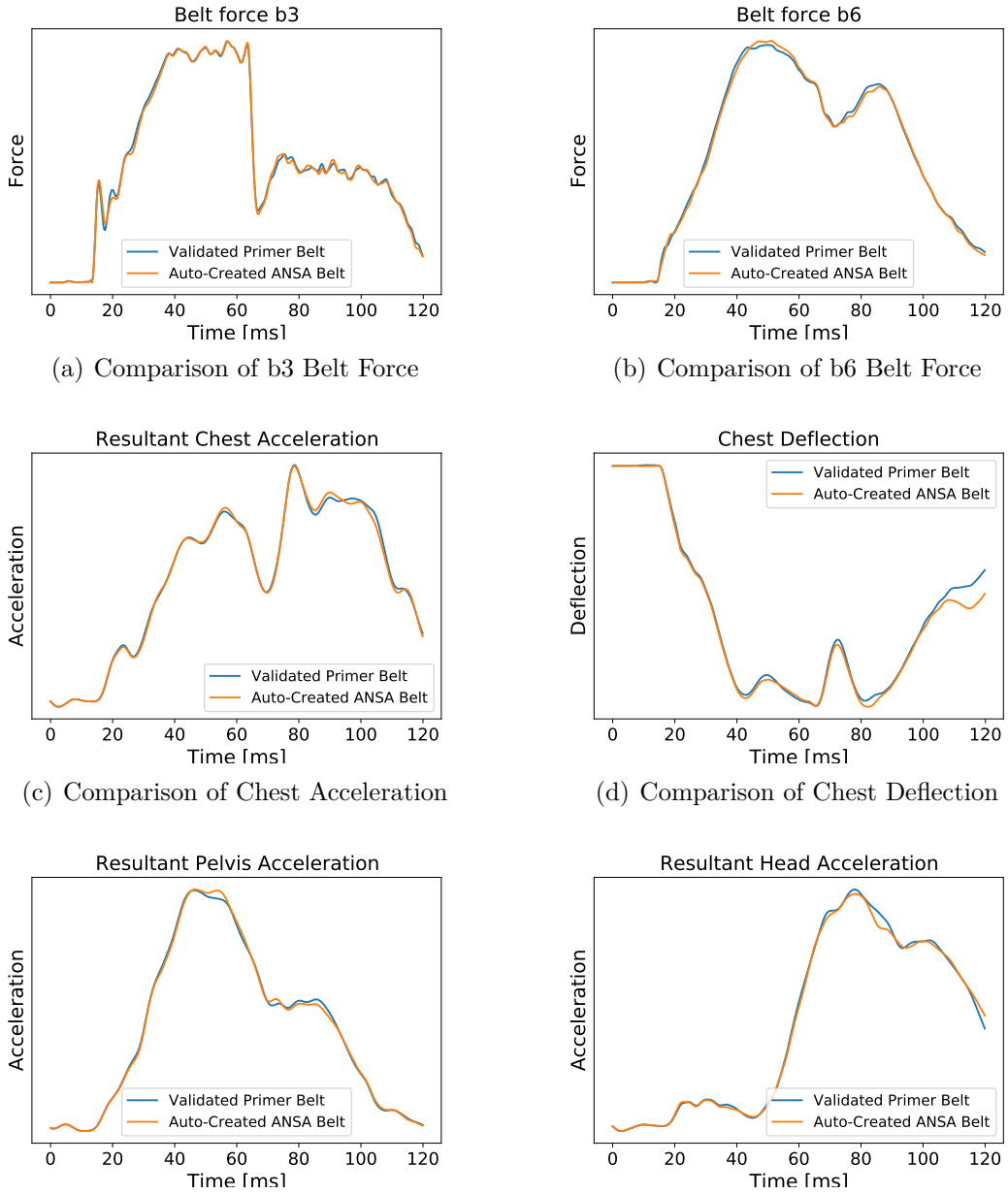

(a) Comparison of b3 Belt Force

(b) Comparison of b6 Belt Force

(c) Comparison of Chest Acceleration

(d) Comparison of Chest Deflection

(e) Comparison of Pelvis Acceleration

(f) Comparison of Head Acceleration

Figure 4.2: Seatbelt created with the Automatic Belt Routing Tool in ANSA in comparison to a validated seatbelt created in the Primer environment

Furthermore, it was found that running the Automated Belt Routing Tool created the exact same seatbelt twice. This not only refers to the properties but also to the belt path even after tensioning the belt. If the two belt models are overlayed, the position of each node and element is an exact representation of the other model.

4.4 Effect of automated routing on the deviation of belt position

To quantify what a natural belt position is to engineers routing a seatbelt on a physical ATD, measurements were taken for ten separate seatbelt routings in the same environment for three different physical ATDs each. These measurements can be observed in Tables 4.1 to 4.3. When comparing the measurement of any physical ATD routing, the dependency of the measurements to each other is evident: A higher M2B results in a lower L2S because they both add up to the distance between Mouth and Lap Belt, which stays approximately the same for each ATD. The M2B also affects the N2S as the N2S increases with the M2B because of the belts diagonal fit on the ATD. Therefore, when analysing the impact of the belt positions the approach can be simplified by only focusing on one measurement, in this case the M2B, as the other measurements change accordingly.

Table 4.1: Belt Position for Humanetics HIII 5^{th}

	Mouth to Shoulder Belt distance	Lap Belt to Shoulder Belt distance	Neck to Shoulder Belt distance	Engineer
1	259.62 mm	131.45 mm	121.97 mm	1
2	269.13 mm	122.37 mm	120.34 mm	1
3	235.58 mm	156.23 mm	96.95 mm	1
4	250.03 mm	141.98 mm	103.40 mm	1
5	269.53 mm	126.64 mm	117.01 mm	2
6	261.52 mm	134.34 mm	108.85 mm	1
7	256.50 mm	137.23 mm	101.73 mm	1
8	259.65 mm	129.67 mm	113.68 mm	1
9	244.99 mm	149.64 mm	101.23 mm	3
10	278.11 mm	117.28 mm	130.14 mm	4

Table 4.2: Belt Position for Humanetics HIII 50^{th}

	Mouth to Shoulder Belt distance	Lap Belt to Shoulder Belt distance	Neck to Shoulder Belt distance	Engineer
1	249.74 mm	212.20 mm	93.47 mm	1
2	308.49 mm	154.08 mm	123.42 mm	1
3	281.05 mm	174.95 mm	109.47 mm	1
4	269.76 mm	191.51 mm	104.42 mm	1
5	273.78 mm	182.24 mm	104.19 mm	1
6	335.24 mm	127.06 mm	140.95 mm	2
7	276.82 mm	185.07 mm	104.43 mm	1
8	271.81 mm	189.87 mm	101.61 mm	1
9	305.94 mm	155.49 mm	125.05 mm	3
10	348.10 mm	110.82 mm	150.47 mm	4

Table 4.3: Belt Position for Humanetics HIII 95^{th}

	Mouth to Shoulder Belt distance	Lap Belt to Shoulder Belt distance	Neck to Shoulder Belt distance	Engineer
1	302.17 mm	188.24 mm	117.88 mm	1
2	307.93 mm	182.12 mm	115.42 mm	1
3	299.57 mm	191.33 mm	116.39 mm	1
4	270.30 mm	219.25 mm	106.48 mm	1
5	265.84 mm	222.33 mm	98.17 mm	1
6	328.77 mm	161.34 mm	133.69 mm	1
7	273.21 mm	217.28 mm	103.94 mm	1
8	309.85 mm	180.48 mm	123.66 mm	1
9	318.04 mm	172.16 mm	131.64 mm	4
10	302.91 mm	185.97 mm	118.28 mm	3

A box plot of the measurements on each physical ATD can be found in Figure 4.3 and a comparison between the respective measurements on the physical ATDs can be found in Figure 4.4. The black boxes mark the area of the 25^{th} to 75^{th} percentile of measurements with the black lines marking the min or max values. The orange line marks the median value with the black cross marking the average.

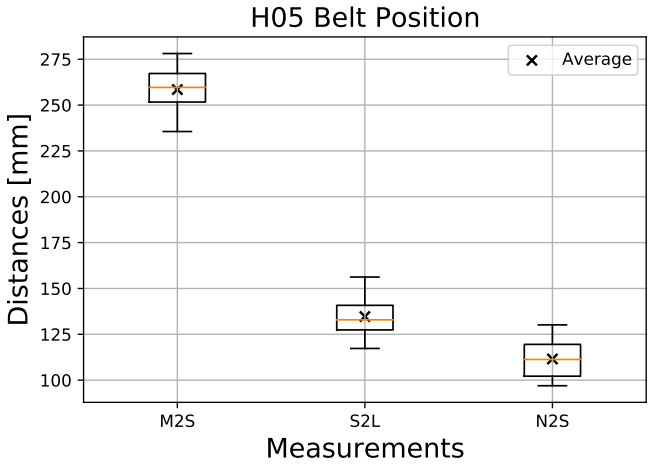

(a) H05 Belt Position

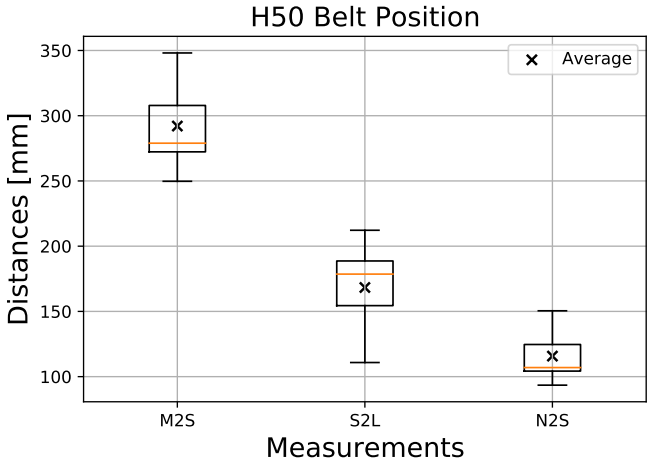

(b) H50 Belt Position

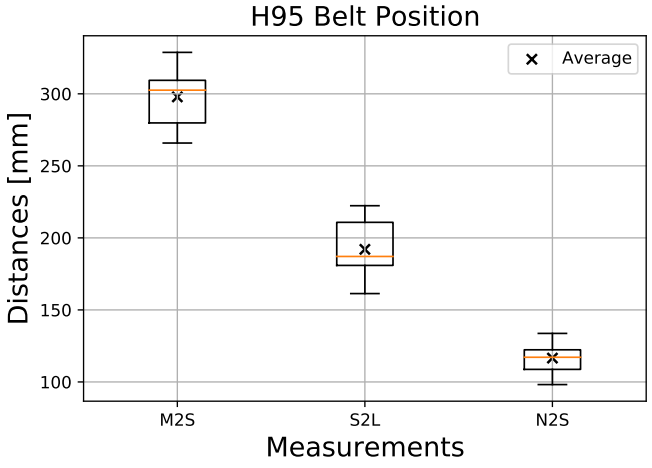

(c) H95 Belt Position

Figure 4.3: Spread of Belt Position after 10 Belt Routings per ATD: Each figure contains all three measurement of the respective dummy displayed as a box plot with the red lines representing the median.

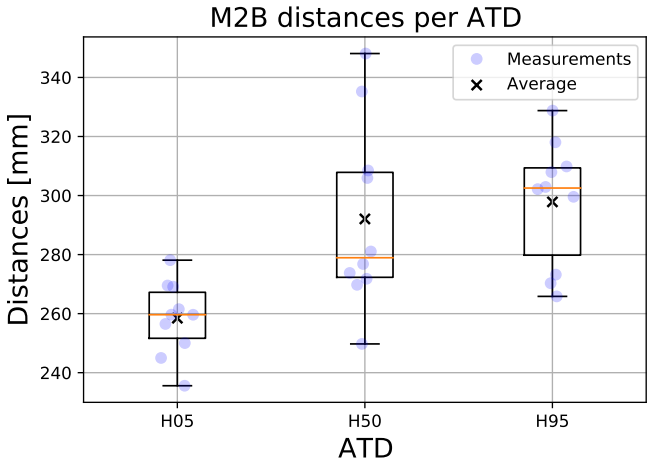

(a) Comparison of Mouth to Belt distances

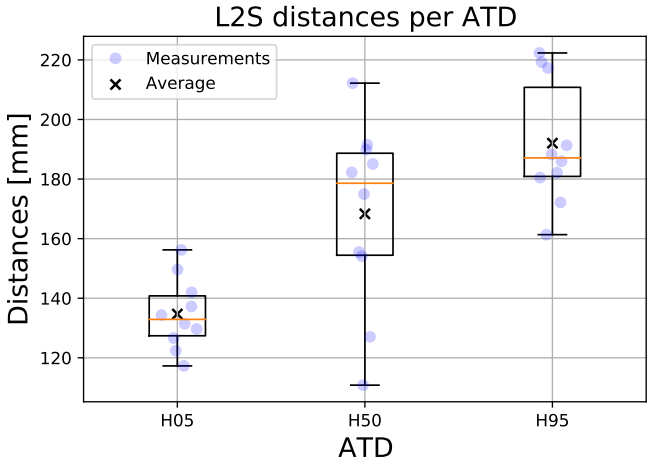

(b) Comparison of Lap Belt to Shoulder Belt distances

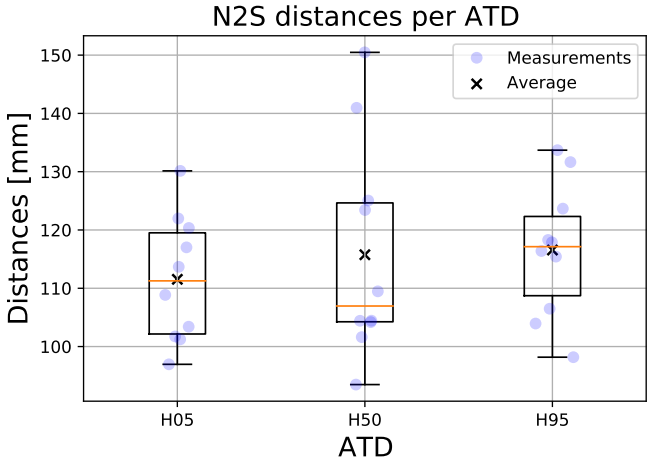

(c) Comparison of Horizontal Neck to Shoulder Belt distances

Figure 4.4: Comparison of box plots of ATD measurements: Each figure contains all three ATD values of the respective measurement displayed as a box plot with the red lines representing the median.

It is noticeable in Figure 4.4(a) that the average M2B seems to approximatly be proportional to the ATD's seated height which is 787.4 mm for the 5^{th} female, 883.9 mm for the 50^{th} male and 919.5 mm for the 95^{th} male. An approximation between M2B for ATDs and their respective seated height l_{sh}) is:

$$M2B \approx \frac{l_{\text{sh}}}{3} \tag{4.1}$$

However, the spread differs between the ATDs as belt position on the 50^{th} male varies the most between the measurements. As Table 4.4 suggests, the spread is mainly due to the subjective feeling for a natural belt position between the 4 engineers, who routed the seatbelt as the average spread was approximatley 40% lower when just Engineer 1 routed the seatbelt. The impact of different engineers routing seatbelt was notably less for the 5^{th} female as well as the 95^{th} male.

Table 4.4: Tabular evaluation and comparison of measurements

	H05	**H50**	**H95**
M2B Average	258.47 mm	292.07 mm	297.86 mm
M2B Average (only Engineer 1)	256.00 mm	275.92 mm	294.71 mm
M2B Spread	42.53 mm	98.36 mm	62.93 mm
M2B Spread (only Engineer 1)	33.55 mm	58.75 mm	62.93 mm
M2B Average Spread	11.89 mm	29.76 mm	20.12 mm
M2B Average Spread (only Engineer 1)	9.87 mm	17.48 mm	21.02 mm

Figure 4.5 shows the subjectivity of a "natural" belt position to different people. While Engineer 1, who routed at least 7 out of 10 belts each time, in average has a shoulder belt position that is increasing proportional to the ATDs seated height. The other three engineers, who each routed only one seatbelt, seem to be impacted by the 50^{th} male's chest size when it comes to their feeling for a good belt position, with Engineer 4 for instance, preferring a very low shoulder belt position throughout all ATDs.

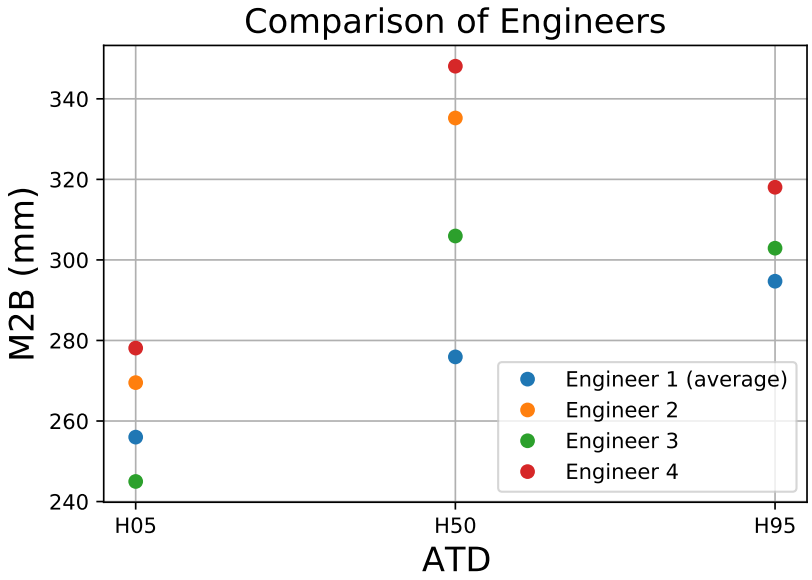

Figure 4.5: Comparison of M2B based on subjective assessment of different engineers for three Humanetics HIII ATDs

4.5 Deviation of belt position on Humans

When comparing the boxplot in Figure 4.6 it is noticeable that the spread on humans is less than on the H50 ATD. The distribution of the values concentrates around the average value resulting in the min and max values often being identified as "outliers". As previously noticed when comparing the ATDs M2B values, the correlation of seated height and M2B is also noticeable when comparing the Human measurements.

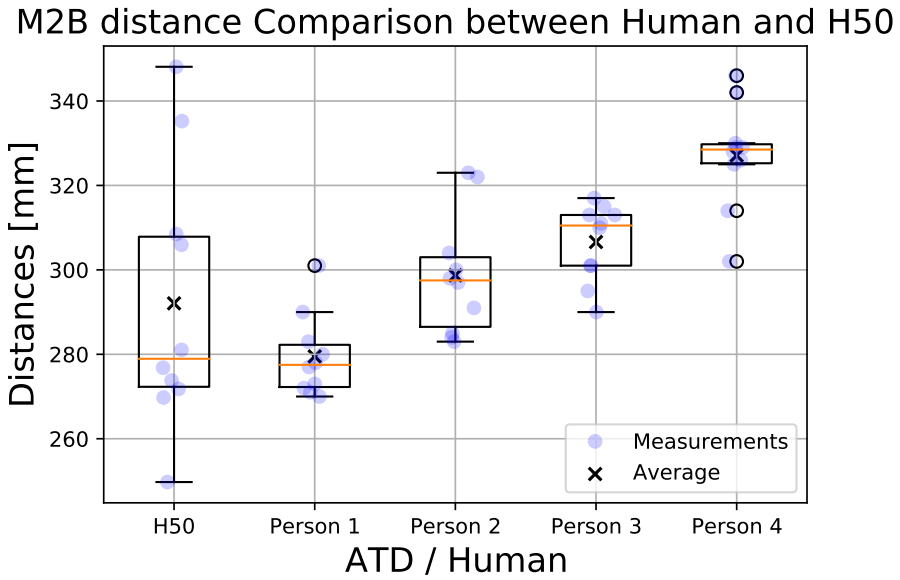

Figure 4.6: Comparison of M2B between Humans and H50. The red line represents the median value.

4.5.1 Influence of belt routing deviation on Humanetics HIII 5^{th} female

Among the ATDs tested, the H05 exhibited the least variation in its shoulder belt position. After simulating the impact of these deviations on MPDB crash test results, most forces, deflections, and other criteria did not show a clear influence from the variation in shoulder belt position. However, the difference in position between the minimum and maximum shoulder belt positions did affect chest compression by approximately 5^{th}, with the lower shoulder belt position resulting in higher chest deflection. Furthermore, it was observed that forces in the lap belt tended to increase as the shoulder belt position elevated as it can be seen in Figure 4.7(b). However, this trend is not very pronounced concerning the peak belt force for the H05 ATD.

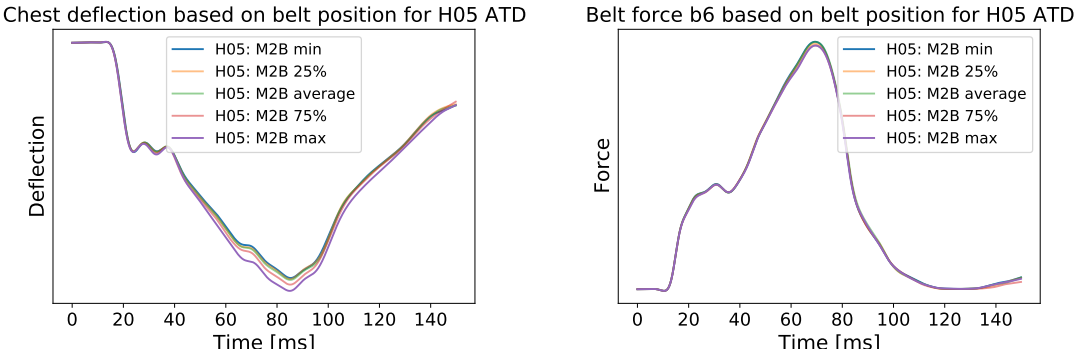

(a) Chest Deflection

(b) Belt Force b6

Figure 4.7: Influence in belt position for H05 ATD

The trend was confirmed by the results of the same model using the 25 mph FFRB crash pulse, which exhibited approximately the same deviations in percentage terms.

4.5.2 Influence of belt routing deviation on Humanetics HIII 50^{th} male

In the 50^{th} male, there was no variation in the quantified simulation results except in the lap belt force and chest deflection. The maximum chest deflection at the lowest belt position was approximately 23% higher than at the highest belt position. It is worth noting that unlike the 5^{th} female, the chest of the 50^{th} male experiences compression for a longer duration. The lowest belt position was also found to load the lap belt about 10% less than the highest shoulder belt position.

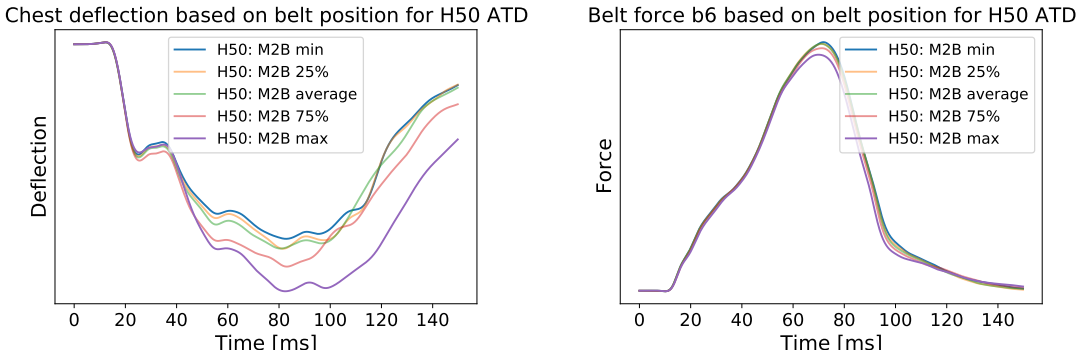

(a) Chest Deflection (b) Belt Force b6

Figure 4.8: Influence in belt position for H50 ATD

The trend was confirmed by the results of the same model using the 25 mph FFRB crash pulse, which exhibited approximately the same deviations in percentage terms.

4.5.3 Influence of belt routing deviation on Humanetics HIII 50^{th} male

Similar to the other two ATDs, the simulation results of the H95 also did not show any notable variation in plots such as Pelvis Acceleration or Head Acceleration. The Chest deflection however showed differences with the lowest shoulder belt position having a maximum deflection that is approximately 20% higher than the maximum chest deflection of the highest shoulder belt position. The forces in the lap belt, as measured in cross section b6 increased as the routed shoulder belt position moved further upwards towards the neck.

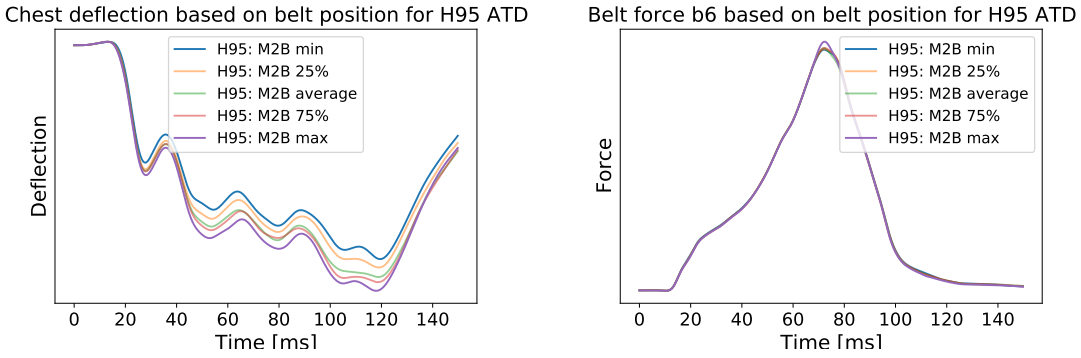

(a) Chest Deflection (b) Belt Force b6

Figure 4.9: Influence in belt position for H95 ATD

The trend was confirmed by the results of the same model using the 25 mph FFRB crash pulse, which exhibited approximately the same deviations in percentage terms.

4.5.4 ATD uncertainty margins

Uncertainty margins were established for chest deflection, identified as the most crucially affected injury criterion, as detailed in Table 4.5. Two uncertainty margins were applied for each of the three Hybrid III ATDs previously utilised. The first margin considered a 50^{th} percentile confidence interval. This approach utilised the peak chest deflection of the average belt position as a reference value, with the deviations in peak chest deflection of the 25^{th} and 75^{th} percentile belt positions serving as upper and lower bounds, respectively. For a more conservative strategy, a second uncertainty margin was formulated using the lowest and highest M2B positions as upper and lower bounds, respectively.

Table 4.5: Chest deflection uncertainty margins for Humanetics HIII ATDs

	H05	**H50**	**H95**
50 percentile boundaries	nominal $^{+2\%}_{-1\%}$	nominal $^{+9\%}_{-0\%}$	nominal $^{+2.2\%}_{-4.2\%}$
100 percentile boundaries	nominal $^{+4.7\%}_{-1\%}$	nominal $^{+20.8\%}_{-4.8\%}$	nominal $^{+6\%}_{-7.7\%}$

4.5.5 Influence of shoulder belt position on SAFER HBM

Simulating a spread in the M2B of 60 mm in 15 mm steps using an MPDB crash pulse on a SAFER HBM seated in Position 4 reveals the influence of shoulder belt position on the ribs that are directly loaded by the belt. As depicted in Figure 4.10, a higher belt position tends to load the upper ribs of the HBM's thorax more heavily. Additionally, the belt position markedly affects the force distribution between the left and right ribs, with the lowest belt position resulting in a predicted rib strain more than twice as high as the higher belt position for Ribs 3 and 4. Moreover, the highest belt position predominantly loads Rib 1 on the right side. Figure 4.11 further illustrates that the primary load shifts from the left rib cage to the right rib cage as the shoulder belt is positioned lower.

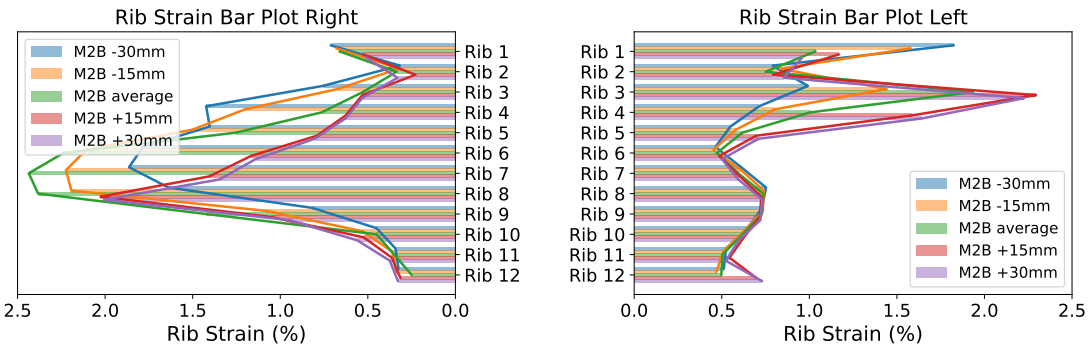

(a) Rib Strain Bar Plot Right

(b) Rib Strain Bar Plot Left

Figure 4.10: Rib Strain Bar Plot for variation of M2B on SAFER HBM

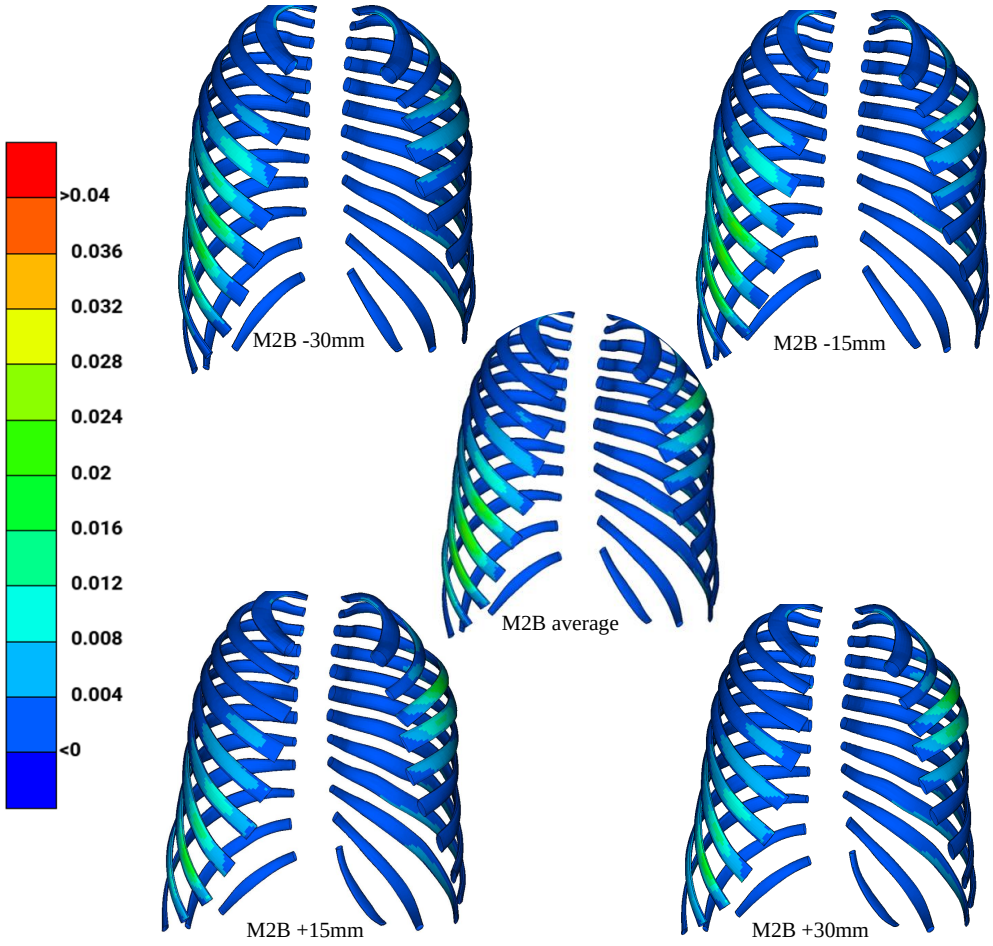

Figure 4.11: Comparison of maximum rib strain in front right rib cage

Table 4.6 shows the predicted risks of rib fractures for age groups of 25-, 45- and 65-year-olds. The risks are based on how likely it is for the occupant of the respective age groups to fracture at least 2, 3 or 4 ribs. When examining the probability of rib fractures across various belt positions and age categories, it becomes apparent that positioning the shoulder belt at the average level poses the highest risk of rib fractures. As the belt deviates further from this position, the probability of occupants experiencing fractures decreases.

Table 4.6: Differences of predicted rib fracture probability between various M2B positions and the baseline in MPDB crash simulations using SAFER HBM

	25 years of age			45 years of age			65 years of age		
	2+	3+	4+	2+	3+	4+	2+	3+	4+
M2B -30	-2%	0%	0%	-21%	-4%	0%	-44%	-33%	-10%
M2B -15	-1%	0%	0%	-12%	-3%	0%	-15%	-15%	-6%
M2B average	Baseline								
M2B +15	-2%	0%	0%	-19%	-4%	0%	-41%	-35%	-11%
M2B +30	-2%	0%	0%	-20%	-4%	0%	-44%	-36%	-11%

To determine if this pattern persists with a different crash pulse, the same model underwent simulation using an FFPD crash pulse. As indicated in Table 4.7, the reduction in impact speed correlated with a decrease in the probability of rib fractures. Nonetheless, the trend of reduced rib fracture probability for a belt position farther from the average position remained consistent.

Table 4.7: Differences of predicted rib fracture probability between various M2B positions and the baseline in FFRB crash simulations using SAFER HBM

	25 years of age			45 years of age			65 years of age		
	2+	3+	4+	2+	3+	4+	2+	3+	4+
M2B -30	0%	0%	0%	-1%	0%	0%	-12%	0%	0%
M2B -15	0%	0%	0%	-1%	0%	0%	-5%	0%	0%
M2B average	Baseline								
M2B +15	0%	0%	0%	-1%	0%	0%	-8%	0%	0%
M2B +30	0%	0%	0%	-1%	0%	0%	-12%	0%	0%

A 0% difference between the baseline and the rib fracture probability for the modified belt position indicates that the occupant is unlikely to sustain a fractured rib in either scenario. This means that the absence of a difference in rib fracture probability cannot necessarily be attributed to the belt position having no impact.

5
Discussion

The developed tool is capable of creating seatbelts with a high degree of automation, minimising the user input. Time-saving is one of its greatest advantages. The ability to create a seatbelt in a very short time allows engineers to work more efficiently and thus increase the rate of improvement in vehicle safety.
Also, the standardisation of seatbelts allows for an improvement in comparability. It has been found that variations in seatbelt position can affect injury criteria. This can lead to incorrect conclusions when comparing simulations. Standardisation enables repeatability and comparability.
The ability to expand automation with minimal effort to additional ATDs, HBMs, and various vehicle models and positions in any combination ensures future usability.
Through various delta studies regarding the influence of different factors, a combination of belt parameters has been developed, representing a balance between practical processing and an accurate representation of average physical routing. Combined with the examination of differing belt positions, expected deviations in simulation or crash test results within a tolerance range can be specified.
Standardisation always comes with the loss of individualisation. While this is beneficial for reproducibility, complete automation may not be suitable for research purposes, as adjusting the belt path would require modifying values in the corresponding CSV file repeatedly. This issue is addressed by developing Custom Routing, which offers the option to create a more individualised belt while retaining time-saving advantages. Thus, the automated seatbelt routing tool is usable for any belt routing use case.

5.1 Validation

A model can never replicate the precise properties of its physical counterpart. It serves as an abstraction, enabling engineers to simulate specific properties in a manner where the model's test results closely approximate those of the physical counterpart. Or as the statistican George E.P. Box put it "All models are wrong, but some are useful" [Box and Draper 1919]. Therefore a good model allows making assessments, such as crash performance, based on the model's outcomes. However, determining whether a model can be considered validated is a challenging task, as numerous influencing factors in the simulation affect the outcome. If one wants to validate the seatbelt of a vehicle in a crash test simulation based on a physical crash, one must first validate the structural elements, the seat, the ATD model, and other subsystems that have a direct or indirect influence.

As an alternative to this approach, the validation claim for the seatbelts created in ANSA was set that these seatbelts should aim for nearly identical performance as validated seatbelts created with the previously used Primer software. This means that the reaction to forces in the vehicle should occur in the same manner at the same time. As Figure 4.2 shows, it is possible to closely replicate belt influenced criterias and thus the belt performance, which is why the seatbelt can be considered validated. The automation exclusively generates the belt webbing along with its associated anchors and properties. Factors such as friction, pretensioning, webbing material, and retractor forces before and during the crash are merely assigned but not created.

5.2 Deviation in Belt Position

The research reveals a notable increase in shoulder belt spread on the H50 Anthropomorphic Test Device (ATD), primarily attributed to varying perceptions regarding how the belt should be routed on this particular ATD. The Humanetics HIII ATDs, designed based on soldier body shapes, exhibit notably muscular characteristics, with the 50^{th} male featuring a chest shape that may seem disproportionately large to many individuals, potentially leading to an unconventional feeling in belt routing. Additionally, it's worth noting that, except for Engineer 1, a greater distance between the mouth and the belt was selected for the 50^{th} male compared to the 95^{th}. The substantial chest size of the 50^{th} male may result in a shoulder belt placement over the chest, creating a sensation of the belt making contact with the neck during frontal impacts, possibly contributing to this observed trend. Conversely, the 5^{th} female exhibited the least spread, likely due to the natural belt guidance provided by the female chest. As the midsection of the female chest serves a concave surface for the belt webbing and the large chest of the 50^{th} male is rather convex, there seems to likely be a dependence between the spread in belt position and the surface shape. A convex surface results in a larger spread while a concave surface results in a lower spread meanin that the belt is likely to end up in a concave area of the human torso. Consequentially, especially larger bodies with a voluminous belly therefore will have a higher spread in belt position and the belt is more likely to slide upwards during normal driving and during a crash.

Another finding is that the average M2B measured increases proportionally to the ATD's seated height. This means that the 5^{th} female has a lower M2B compared to the 95^{th} male due to its lower seated height. It was found that the M2B is about a third of the seated height.

Experimental uncertainty is a critical consideration in belt routing and its measurements. While it is nearly impossible to entirely prevent human bias and the temptation to manipulate or influence the spread in belt position, it was minimised in this study through meticulous observation. The test results appear to be minimally impacted by human bias, rendering the retrieved data valuable. Given that the measurements were conducted by scanning the seatbelt and its surroundings using state of the art technology and employing CAE for data collection, the precision of the measurements can be considered high.

5.3 Effect of deviation in belt position on Humanetics HIII ATDs

The findings indicate that the initial position of the belt has an impact on the chest deflection of the ATD. Particularly, larger ATDs exhibited a range of ±5% to ±10% in chest compression compared to the average belt position. It was found that the lowest M2B that was retrieved from the collected data resulted in the highest peak chest deflection. Further investigations indicated that this phenomenon likely arises because this particular shoulder belt position aligns most effectively with the sternum of the ATD, thereby exerting the most direct influence on the chest deflection measurement mechanism. This occurs because chest deflection is measured at a specific point, resulting in a lower chest deflection for seatbelts that are routed above or below the measuring device. Variations in seatbelt position can alter crash test outcomes, thereby influencing safety ratings. Additionally, the study uncovered that the shoulder belt position does not notably impact spinal, head, or pelvic accelerations and forces. However, it does affect the force distribution of both the lap and shoulder belt, with the shoulder belt exerting greater force when positioned nearer to the ATD's center of gravity. Predicting a general deviation in belt position for crash simulations and belt model creation is challenging, as it heavily relies on internal processes and guidelines governing belt modeling. Organisations with precisely defined nodes and parameter combinations tend to have minimal deviations, ensuring fully reproducible belt models. Conversely, belts modeled based on engineering judgment with subjective decisions regarding the belt path are likely to exhibit variations similar to those found in physical routing. Additionally, numerous parameters and friction values influence seatbelt performance, further complicating the reproducibility of simulation results. Developing a tool that automates and standardises belt modeling offers engineers the advantage of producing reproducible belts, leading to crash simulation results dependent solely on numerical reproducibility of the entire vehicle and occupant model aswell as solving the corresponding numerical problem. This standardisation is essential for car manufacturers to prepare for crash test ratings and compare different vehicle models without being influenced by variations in belt position.

5.4 Effect of deviation in belt position on SAFER HBM

The results in chapter 4.5.4 show that the SAFER HBM is sensitive to a deviation in the belt position. Even small changes of 15 mm in the M2B showed a reduction in predicted rib fracture probability of 41% for the 65-year age group. It is notable that the average belt position bears the highest predicted probability of rib fractures as the risk decreases the further the belt is moved away from this position within the chosen spread boundaries in both directions. Observations of the FE simulation indicate that for lower shoulder belt positions the HBM's upper torso tends to slightly roll over the belt, not absorbing its full mass inertia at once, distributing

the load over time and into friction. Furthermore, the maximum rib strain plot reveals a higher strain on ribs three to five on the left side, resulting in a more even distribution on the rib cage sides. Additionally, it is likely that the strain in the lower ribs increases at a lower rate when being compressed than it is the case for the higher ribs. The reason for this is likely that the the cartilage which is a connector of the ribs to the sternum, is larger for the lower ribs and therefore takes up more deformation energy. As the shoulder belt position rises over the average, the HBM experiences less forward movement relative to the vehicle resulting in improved restraint despite having a reduced predicted rib fracture risk. This results from a lower momentum of the torso over the belt, which transfers more force to the lap belt. Additionally, with the body having a more upright position, strain on higher ribs is increased. Both leads to an load distribution away from the critical lower right ribs seven and eight. However, it's noted that an even higher belt could potentially increase the strain on the first rib on the left side to a level being most influential so that the predicted rib fracture risk rises again. Especially considering HBMs being used for assessing crash ratings in the near future, the sensitivity of the predicted rib fracture probability to the M2B of the shoulder belt is something that needs to be considered as it can easily influence the test results. An increased probability of multiple rib fractures can quickly change the crash performance according to the Abbreviated Injury Scale (AIS) scale displayed in figure 5.1.

AIS Skeletal injury	
1	One rib fracture
2	Two rib fractures; sternum fracture; pneunothorax
3	Three or more rib fractures on one side; hemothorax; fractures with flail
4	Four or more rib fractures on each of tqo sides; four or more rib fractures with hemo- or pneumothorax
5	Bilateral flail chest

Figure 5.1: AIS rankings for skeletal rib injuries [Schmitt et al. 2019]

The sensitivity of HBMs chest injury criterias is especially critical as they will be part of Euro-NCAP testings in the near future. In order for test results to be meaningful and reproducible, a standardisation of the seatbelt placement is crucial.

5.5 Limitations

The automation is designed to be generic, allowing the CSV file, which serves as the basis for automation, to be expanded as needed. Additionally, seatbelt creation works for ATDs of any size and shape, as well as for HBMs. Therefore, the functionality of the tool has been evaluated for the SAFER HBM and the Humanetics HIII

family but is likely to work for various other ATDs and HBMs aswell. As for the vehicle model, the automation is based on existing models from the specific manufacturer and may therefore not be applicable with other OEM's FE environments. Standardisation has been developed based on seatbelt models of current and past vehicle models, enabling seatbelt creation in these models and likely future ones. However, if the framework around the seatbelt model and thus the requirements for the seatbelt itself change, adjustments may need to be made outside the scope of standardisation, requiring modifications to the script. Furthermore, the automation was developed for ANSA version 24.0.1. While care was taken to use ANSA-specific functions and commands that are as new and durable as possible, their functionality cannot be guaranteed indefinitely.
Validating seatbelts is a complex issue because the model can only be validated if every vehicle component preceding it has been validated. Factors such as friction, deviations in the crash pulse, or simplifications in material junctions affect the overall system, making it impossible to validate the seatbelt as a subsystem based on a physical seatbelt.
In the investigation of the spread in belt position, common Humanetics HIII ATDs were measured on the rear seat of a large SUV. While the choice of vehicle and position was explicitly made to achieve as universally representative measurement results as possible, it should be assumed that deviating D-ring positions, differing pelvis angles, and other vehicle dimensions may slightly influence the measurements and possibly the spread.
The same applies to the measurements with the four human occupants. Additionally, it should be noted that the four participants were selected to compare to the H50, resulting in a very small and homogeneous sample, as this part of the study did not include females or children.

5.6 Future Work

This study found that the M2B has an influence on chest injury criteria for both ATDs and HBMs. To get reproducible physical crash tests a standardisation of the M2B would be necessary. This study shows a method as well as results for a standardised M2B. However, this method was limited to only one seat position in one specific verhicle with one seat configuration per ATD. This approach therefore offers results for this exact configuration which are likely to change in a different environment. Therefore to deliver an accurate approach to finding the expected average M2B for various occupant surrogates in vehicle environments, a large scale study would need to be conducted. In this study various ATDs should be positioned in different seats with different seat angles and therefore different pelvis angles. Additionally, the effect of varying D-Ring positions can be investigated. To also base this study on the human shape in order for it to comply with future crash testings using HBMs, human participants of different shapes and sizes would also need to be included in this study. With the collected information of this future study, reproducibility and an improvement in comparability for physical tests can be achieved. However, this bears the risk of car manufacturers focussing and improving this specific belt position while compromising the safety of deviating belt positions.

6
Conclusion

The automation tool developed in ANSA ensures precise and reproducible positioning of seatbelts, allowing for standardisation and control over deviations in belt routings. This facilitates more efficient and accurate analysis of predicted injury risk, as inconsistencies in seatbelt modeling no longer affect the comparability of crash simulations.
This study presents the development of a tool capable of generating fully reproducible seatbelt FE-models for crash simulation. Additionally, it explores the impact of the initial spread in shoulder belt position following seatbelt routing in physical setups, using three ATDs from the Humanetics HIII family and four human participants. The investigation reveals that the spread in initial belt position varies depending on the size and shape of the ATDs, particularly increasing for larger occupants with a convex surface area. On average, a spread of approximately ± 30 mm in the vertical distance between the occupant's mouth and shoulder belt can be expected.
By replicating these belt positions, the study observes a notable effect on the chest deflection of ATDs, directly influencing the chest injury criteria. This spread leads to deviations in chest deflection for ATDs compared to the baseline, which was the average belt position. Additionally, the impact of belt position was examined on the SAFER HBM, as crash tests involving HBMs are stated to become part of Euro NCAP's testing in the future. A uniform shoulder belt position, as it is achievable with the developed automatic belt positioning tool, is essential for reproducible test results. Furthermore, the FEM results showed that modifying the shoulder belt's path vertically has an influence on the lateral load shift as well as the occupant surrogate's predicted maximum rib strain. The M2B is therefore a factor in interior safety that needs to be considered when creating seatbelt models and running FEM crash test simulations.

References

Beta-CAE-Systems S.A. (2024a). *ANSA Pre-processing*. Brochure.

– (2024b). *Dummy Positioning & Restraining*. Brochure.

Box, G. E. and N. R. Draper (1919). "Essentially, all models are wrong, but some are useful". In: *Statistician* 3.28, p. 2013.

Daniel, K. (2015). "Make cities and human settlements inclusive, safe, resilient and sustainable". In: *UN Chronicle* 51.4, pp. 26–27.

Defensive-Driving (2016). *A History of Seat Belts*. `https://www.defensivedriving.com/blog/a-history-of-seat-belts/`. Accessed: 2024-03-05.

European New Car Assessment Programme (2020). "Data format and Injury Criteria Calculation". In.

– (Nov. 2021). *European New Car Assessment Programme (Euro NCAP) Full Width Frontal Impact Testing Protocol*. Tech. rep. Version 1.2.1.

– (2023). *Adult Occupant Protection*. `https://www.euroncap.com/en/car-safety/the-ratings-explained/adult-occupant-protection`. Accessed: 2024-03-01.

European Union (2019). *Regulation (EU) 2019/2144 of the European Parliament and of the Council of Ministers*.

Febres, J. D. et al. (2020). "Influence of seat-belt use on the severity of injury in traffic accidents". In: *European transport research review* 12.1, pp. 1–12.

Forman, J. L. et al. (2012). "Predicting rib fracture risk with whole-body finite element models: development and preliminary evaluation of a probabilistic analytical framework". In: *Annals of Advances in Automotive Medicine/Annual Scientific Conference*. Vol. 56. Association for the Advancement of Automotive Medicine, p. 109.

Foster, J. K., J. O. Kortge, and M. J. Wolanin (1977). "Hybrid IIIa biomechanically-based crash test dummy". In: *SAE transactions*, pp. 3268–3283.

Fransén, I. and K.-J. Larsson (2015). "Prerequisites for a generic rear seat test rig". In.

Fraunhofer-Gesellschaft (May 2019). *Virtual human body models supplement crash test dummies*. `https://www.fraunhofer.de/en/press/research-news/2019/`

may/virtual-human-body-models-supplement-crash-test-dummies.html. Accessed: Accessed: 2024-03-01.

Friswell, M. I. et al. (1995). *Finite element modelling*. Springer.

Gursel, K. and S. Nane (2010). "Non-linear finite element analyses of automobiles and their elements in crashes". In: *International journal of crashworthiness* 15.6, pp. 667–692.

Humanetics (2017). "User Manual: Humanetics Hybrid III 50th Male". In.

– (2023). *Hybrid III 50th Male*. https://www.humaneticsgroup.com/products/anthropomorphic-test-devices/frontal-impact/hybrid-iii-50th-male/hybrid-iii-50th-male. Accessed: 2024-03-01.

Kahane, C. J. (2018). *A preliminary comparison of seat belt use coded in crash databases and reported by event data recorders*. Tech. rep.

Larsson, K.-J., A. Blennow, et al. (2021). "Rib cortical bone fracture risk as a function of age and rib strain: updated injury prediction using finite element human body models". In: *Frontiers in bioengineering and biotechnology* 9, p. 677768.

Larsson, K.-J., J. Östh, et al. (2024). "A First Step Toward a Family of Morphed Human Body Models Enabling Prediction of Population Injury Outcomes". In: *Journal of Biomechanical Engineering* 146.3.

Leledakis, A. et al. (2023). "Influence of an Individualised Shoulder Belt Position for Diverse Occupant Anthropometries on Seatbelt Interaction in Frontal and Side Impacts". In.

Livermore Software Technology Corporation (2024). *LS-DYNA Manual*. Livermore Software Technology Corporation. Livermore, CA, USA. URL: https://www.dynasupport.com/manuals/ls-dyna-manuals/ls-dyna_manual_volume_i_r13.pdf.

Makris, M., K. Bohman, and A. Osvalder (2023). "Comparison of Sitting Postures and Shoulder Belt Fit of Rear Seat Car Passengers Over Time in Stationary and Driven Scenarios". In: pp. 690–707.

NHTSA, N. H. T. S. A. (2024). "Seat Belts". In.

Östh, J. et al. (2021). "Numerical reproducibility of human body model crash simulations". In: pp. 431–441.

Pereira, N. Q. and B. Callaghan (2013). *A Comparison New Car Assessment Program NCAP Requirements and Procedures Around the World*. Tech. rep. SAE Technical Paper.

Ratingen, M. van (2020). "Update on Virtual Testing in safety assessment of new vehicles from Euro NCAP". In: *IRCOBI pre-conference workshop VIRTUAL-OSCCAR Workshop: Progress in Virtual Testing for automotive applications*. Vol. 8.

Reed, M. P., S. M. Ebert, and J. J. Hallman (2013). *Effects of driver characteristics on seat belt fit*. Tech. rep. SAE Technical Paper.

Reed, M. P., S. M. Ebert-Hamilton, and J. D. Rupp (2012). "Effects of obesity on seat belt fit". In: *Traffic injury prevention* 13.4, pp. 364–372.

SAFER (2022). *SAFER Human Body Model*. `https://www.saferresearch.com/news/safer-human-body-model-going-global-save-more-lives-traffic`. Accessed: 2024-04-29.

Schmitt, K.-U. et al. (2019). *Trauma biomechanics: an introduction to injury biomechanics*. Springer.

Seattle Safety (2018). *Seattle Safety ServoSled Catapult Sled Systems*. Accessed: 2024-03-01. URL: `https://www.tesscorn-analysis.com/wp-content/uploads/2018/01/Seattle-Safety-ServoSled-Catapult-Sled-Systems.pdf`.

Shah, C. et al. (2014). "Newly developed LS-DYNAő models for the THOR-M and harmonized HIII 50th crash test dummies". In.

World Health Organization (2016). *Global status report on road safety 2015*. Tech. rep. World Health Organization.

– (2023). *Global status report on road safety 2022*. Tech. rep. World Health Organization.

Xu, T. et al. (2018). "Development and validation of dummies and human models used in crash test". In: *Applied bionics and biomechanics* 2018.

DEPARTMENT OF MECHANICS AND MARITIME SCIENCES
CHALMERS UNIVERSITY OF TECHNOLOGY
Gothenburg, Sweden 2024
www.chalmers.se